Innate cortical gradients constrain cross-modal plasticity

Marco Tamietto

marco.tamietto@unito.it

University of Torino https://orcid.org/0000-0002-8815-8499

Davide Orsenigo

University of Turin

Francesca Setti

IMT School for Advanced Studies Lucca

Marco Pagani

IMT School for Advanced Studies Lucca

Giovanni Petri

Northeastern University London

Andrea Luppi

Department of Psychiatry, University of Oxford

Emiliano Ricciardi

IMT School for Advanced Studies Lucca https://orcid.org/0000-0002-7178-9534

Article

Keywords:

Posted Date: September 3rd, 2025

DOI: https://doi.org/10.21203/rs.3.rs-7442112/v1

Additional Declarations: There is **NO** Competing Interest.

Innate cortical gradients constrain cross-modal plasticity

Davide Orsenigo,[1,2,*] Francesca Setti,[3,*] Marco Pagani,[3] Giovanni Petri,[4,5,2,†] Marco Tamietto,[1,6,†] Andrea I. Luppi,[7,8,9,†] and Emiliano Ricciardi[3,†]

[1] *Department of Psychology and Neuroscience Institute of Turin (NIT), University of Torino, Turin, Italy*
[2] *NPLab, CENTAI Institute, Turin, Italy*
[3] *MOlecular MInd LAB, IMT School for Advanced Studies Lucca, Lucca, Italy*
[4] *NPLab, Network Science Institute, Northeastern University London, London, United Kingdom*
[5] *Department of Physics, Northeastern University, Boston, USA*
[6] *Department of Medical and Clinical Psychology, Tilburg University, Tilburg, The Netherlands*
[7] *Department of Psychiatry, University of Oxford, Oxford, United Kingdom*
[8] *St John's College, University of Cambridge, Cambridge, United Kingdom*
[9] *Montréal Neurological Institute, McGill University, Montréal, QC, Canada*

(Dated: August 22, 2025)

Innate cortical organisation and postnatal sensory experience interact dynamically to shape the functional architecture of the human brain. Using naturalistic stimulation, functional gradient analyses, and comparative approaches in congenitally blind, congenitally deaf, and typically developed individuals, we investigate how intrinsic hierarchical structures and sensory experiences influence cortical organisation. Our findings demonstrate that the principal functional gradients spanning from unimodal sensory to transmodal association cortices are consistently preserved across all groups, suggesting a robust genetically determined cortical scaffold. Nonetheless, congenital sensory deprivation selectively reshapes the geometry of modality-specific gradients, characterised by reduced functional differentiation within sensory-deprived cortical regions. These geometric contractions promote experience-driven plastic reorganization, enabling deprived sensory areas to establish enhanced functional connectivity with transmodal and non-deprived sensory cortices. Critically, this reorganisation aligns systematically with pre-existing cortical gradients, highlighting intrinsic hierarchical constraints that guide experience-dependent plasticity. Moreover, sensory-deprived regions exhibiting heightened connectivity actively engage in processing structured perceptual information from intact modalities, reflecting specific feature-driven cross-modal adaptations. Collectively, these results underscore a fundamental duality in cortical organisation: innate hierarchical principles impose constraints on cortical architecture, while sensory experience drives adaptive refinement, demonstrating the brain's intrinsic capacity for flexible functional reconfiguration in response to sensory deprivation.

Understanding how sensory experience shapes brain development and functional organisation is central to neuroscience, bridging two long-standing theoretical perspectives. One view emphasises genetically encoded constraints as primary determinants of brain architecture [1, 2], while the other underscores the importance of experience-dependent plasticity in refining and adapting neural systems throughout development [3–5]. Although intrinsic structural and functional features of cortical organisation are evolutionary conserved across individuals and species, implying foundational principles of cortical architecture [6, 7], sensory experience significantly shapes the maturation and specialisation of neural circuits, particularly within modality-specific systems [8–10]. This dynamic interplay between genetic predispositions and sensory experience becomes particularly evident in cases of early sensory deprivation, where substantial cortical reorganisation and connectivity provides unique insights into how experience modulates the development of large-scale neural networks [10–13].

Traditionally, investigation into brain organisation has primarily relied on discrete regional analyses and pairwise interactions under physiological or pathological conditions. However, recent advances underscore the importance of conceptualising the brain as a complex, economically optimised system operating across multiple spatial and temporal scales [14–18]. A significant limitation of region-based approaches lies in their inability to capture the flexible, context-dependent engagement of both primary sensory and higher-order transmodal cortices [19, 20]. In contrast, models describing cortical organisation along continuous gradients — from unimodal sensory regions to transmodal integrative areas — have garnered substantial empirical support, reflecting the brain's inherent structural and functional heterogeneity [21–24].

Yet, the notion of cortical "hierarchy" itself encompasses diverse interpretations, including serial information flow, topological embedding, specialisation gradients, and developmental trajectories[25]. Converging evidence indicates that low-dimensional functional gradients, particularly a principal one extending from primary sensory/motor to higher-order transmodal cortices, effectively capture this multifaceted hierarchical architecture [26–35]. Notably, this principal gradient aligns with core developmental, evolutionary, and functional brain properties, such as prolonged postnatal maturation and pro-

* These authors contributed equally
† Co-senior authors

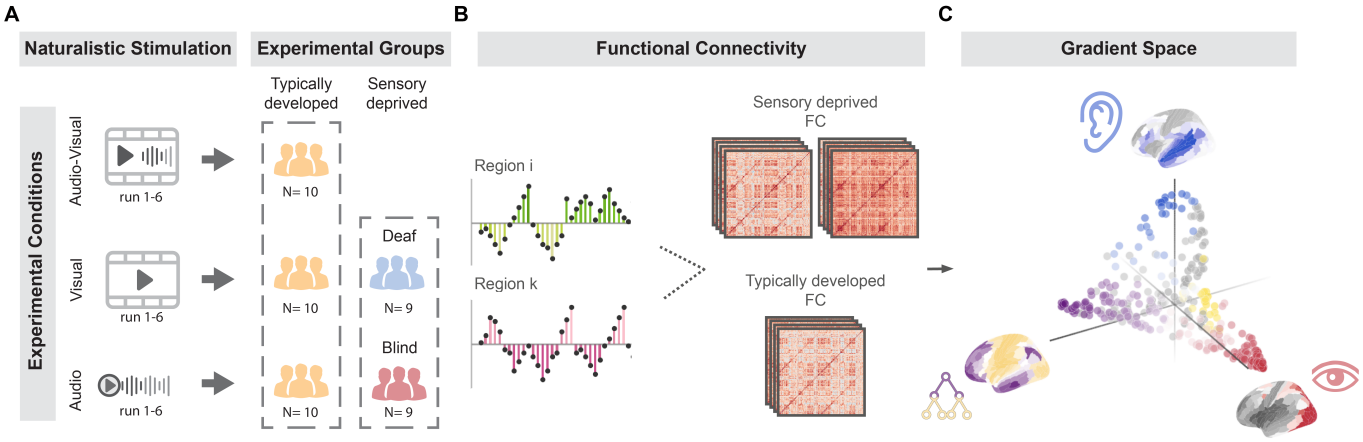

Figure 1. **Experimental Paradigm and Data Analysis Pipeline. A,** Participants viewed six runs of a naturalistic movie (*101 Dalmatians*) presented in three sensory formats: audiovisual, visual-only, and audio-only. The design included three groups of typically developed participants (N=10 per condition) and two groups of congenitally sensory-deprived individuals: blind (N=9) and deaf (N=8). **B,** Functional connectivity (FC) was computed from BOLD signals recorded via fMRI during movie viewing. FC matrices were estimated for each group and condition to examine pairwise regional interactions. **C,** Diffusion embedding was applied to the FC matrices to derive low-dimensional cortical gradients. These gradients were used to assess the global functional architecture and determine how congenital sensory deprivation affects its spatial geometry and hierarchical organization.

gressive cortical specialization, supporting the emergence of higher-order cognition [27, 36].

While extensive research has characterised features of the principal gradient, how secondary gradients emerge and their modulation by sensory experience remain unclear. Empirical studies in congenitally blind or deaf individuals suggest that large-scale functional architectures can develop even without modality-specific sensory inputs (e.g. Ricciardi *et al.* [37, 38], Setti *et al.* [39], Lettieri *et al.* [40]), pointing to intrinsic scaffolds anchored in cortical geometry and structural connectivity [41, 42]. Nevertheless, how experience-dependent mechanisms refine or reorganise these gradients, especially under sensory deprivation, remains unresolved [43].

To address this question, we analysed data from congenitally blind, congenitally deaf, and neurotypically developed participants presented with naturalistic stimuli (movie-watching of *101 Dalmatians* [39]). Ecologically rich paradigms, such as full movies, engage the full spectrum of sensory modalities and cognitive functions, including social cognition, narrative comprehension, and higher-order reasoning, thereby providing enhanced ecological validity compared to resting-state or simplified tasks [44, 45]. Indeed, recent evidence indicates that naturalistic viewing is uniquely suited to capturing the functional granularity of cortical gradients, as it evokes context-specific neural states and brain dynamics[44]. This unique dataset enabled us to address two critical questions: (i) can cortical gradients emerge in the absence of modality-specific sensory input? and, (ii) How does sensory deprivation impact the spatial structure and functional specificity of these gradients?

We find that –while the fundamental hierarchical scaffold remains preserved regardless of sensory experience– deprivation leads to reduced specificity within the affected modality and fosters compensatory connectivity re-routing involving preserved unimodal and transmodal regions. Collectively, these results highlight a dynamic interplay between innate cortical architecture and experience-dependent plasticity, suggesting that functional gradients are neither entirely hardwired, nor wholly experience-driven.

RESULTS

Gradient topography during processing of naturalistic auditory, visual and audiovisual processing in typically developed individuals

To characterise the macroscale functional architecture of the cortex under naturalistic stimulation, we computed pairwise functional connectivity (FC) matrices from regional BOLD time series, separately for each experimental group and condition. We then applied diffusion map embedding [46, 47] - a non-linear dimensionality reduction technique akin to principal component analysis (PCA;[16, 26, 48]) – to the group-level FC matrices to extract cortical gradients (Figure 1). We focused on the first three gradients, as they represent the primary hierarchical dimensions of functional organisation, spanning from unimodal sensory areas to transmodal association networks [26, 49].

Qualitative inspection of the extracted gradients revealed both shared structures and condition-specific topographies across experimental groups (Figure 2, see also Figure S1,S2). Gradients derived from unimodal and multimodal naturalistic stimulation both reflect the

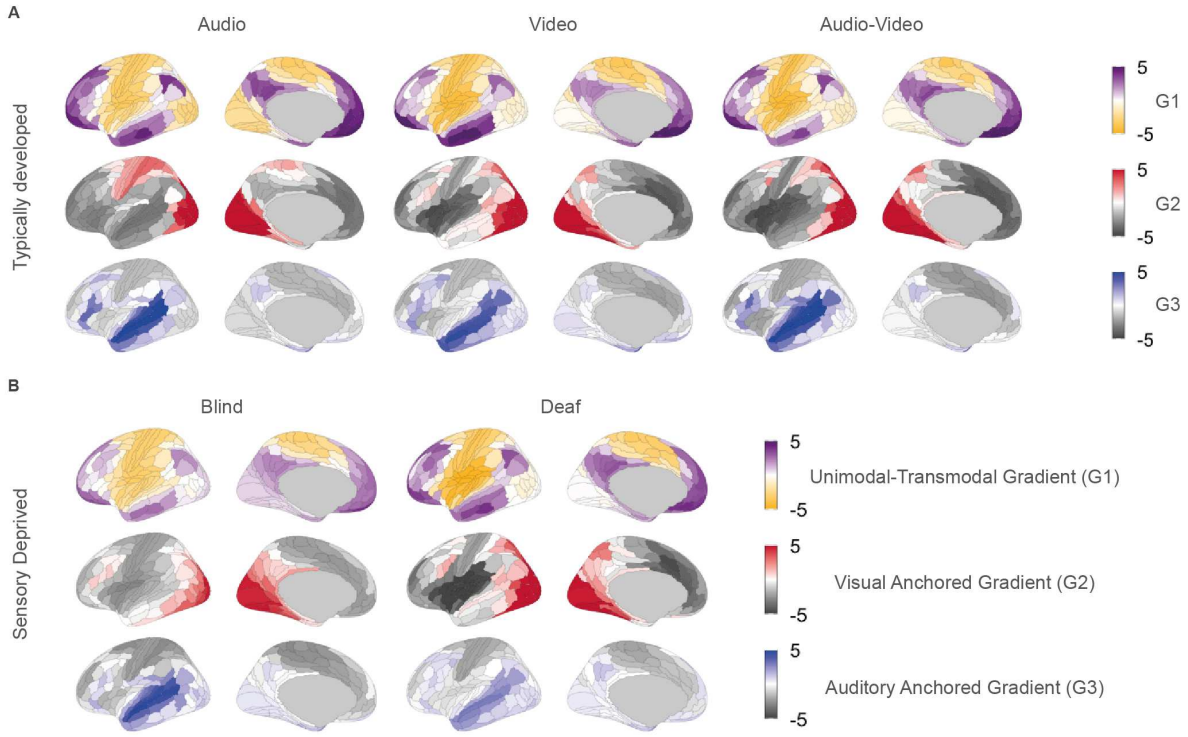

Figure 2. **Topographical maps of functional gradients across groups and conditions. A,** Surface representations of the first three cortical gradients are shown for typically developed participants under three naturalistic stimulation conditions: audio-only, visual-only, and audiovisual. Gradient 1 (G1) captures the principal unimodal-to-transmodal axis, while Gradient 2 (G2) and Gradient 3 (G3) are anchored in visual and auditory cortices, respectively. **B,** Corresponding gradient maps are shown for congenitally blind and congenitally deaf individuals, collapsed across sensory conditions. In both sensory-deprived groups, G1 remains consistent with the canonical cortical hierarchy, while G2 and G3 exhibit altered spatial differentiation, reflecting the absence of modality-specific experience..

canonical macroscale organisation of cortical hierarchy, and capture condition-dependent functional architectures. Consistent with prior findings [44], the embedding spaces under naturalistic stimulation showed enhanced differentiation along modality-specific axes, particularly within the visual and auditory systems (Figure 2A). The first gradient (G1) consistently reflects the canonical sensorimotor-to-transmodal cortical hierarchy across all conditions, mirroring intrinsic organisational principles also observed at rest [44]. However, in contrast to generalised embedding reported during rest, naturalistic stimulation elicited modality-specific refinements. During audiovisual and visual conditions, the second (G2) and third (G3) gradients were anchored in visual and auditory cortices, respectively, indicating the emergence of modality-specific granularity atop the preserved canonical structure. These findings suggest that naturalistic stimulation evokes distinct, context-sensitive cortical geometries, where dominant sensory modalities sculpt the expression of secondary gradients. Altogether, these results demonstrate that while the major organisational axes of the cortex are conserved across conditions, their relative prominence and spatial specificity are modulated by the sensory context. This indicates that functional gradients are dynamically shaped by naturalistic input.

Sensory deprivation preserves gradient topography but reshapes functional cortical geometries

Building on our findings in neurotypically developed individuals, we next investigated how congenital sensory deprivation affects the expression and geometry of cortical gradients under naturalistic stimulation. If cortical gradients are intrinsically hardwired, they should be preserved regardless of sensory input. Alternatively, if postnatal experience is a constitutive prerequisite for shaping cortical organisation, we would expect marked differences in gradient structure under sensory deprivation. Our results reveal that the global hierarchical organisation of cortical gradients is largely preserved in both congenitally blind and deaf individuals. Specifically, the first three gradients consistently map onto a unimodal-to-transmodal axis (G1), a visually anchored axis (G2), and an auditory anchored axis (G3), respectively (Figure 2B). This preservation indicates that the macroscale

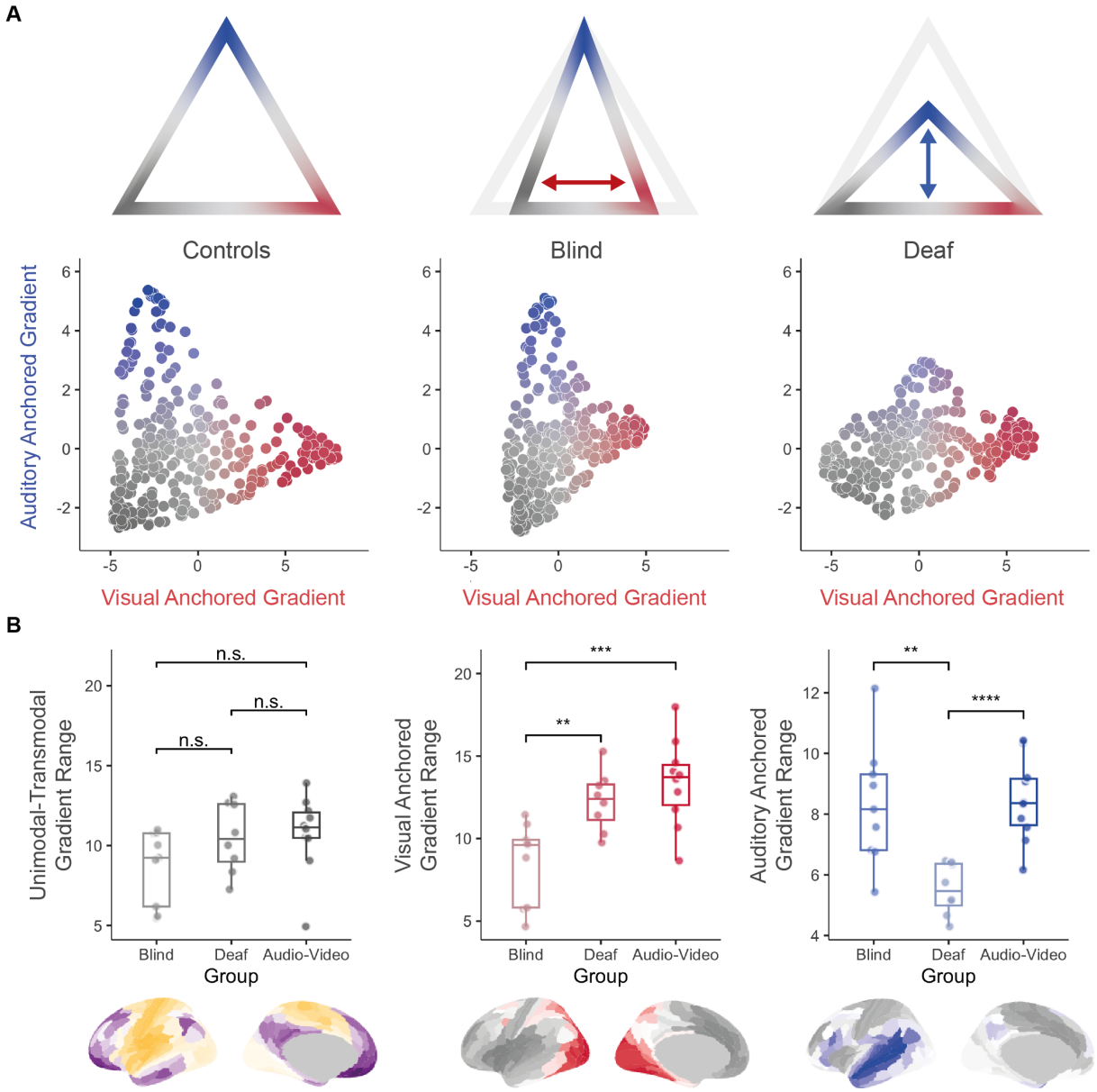

Figure 3. **Functional geometry reconfiguration under sensory deprivation. A,** Two-dimensional scatter plots illustrate the spatial embedding of cortical regions along the visual-anchored (G2) and auditory-anchored (G3) gradients in typically developed (audiovisual condition), congenitally blind, and congenitally deaf participants. The top panel schematically highlights the observed contraction patterns: visual gradient compression in blind individuals (horizontal arrow) and auditory gradient compression in deaf individuals (vertical arrow). **B,** Boxplots show gradient range values for the three groups along the first three functional gradients. No significant differences are observed for the unimodal-to-transmodal gradient (G1). In contrast, significant reductions in the visual gradient range (G2) are found in blind participants and in the auditory gradient range (G3) in deaf participants, compared to the typically developed group under audiovisual stimulation. Statistical comparisons are based on two-tailed t-tests with FDR BH correction (n.s. = not significant; ** $p < 0.01$; *** $p < 0.001$; **** $p < 0.0001$). Gradient maps below each plot depict the corresponding spatial topography.

scaffold of cortical functional geometry is established independently of modality-specific sensory experience.

However, we observed significant differences in the geometric properties of this low-dimensional embedding space (Figure 3A). To do this, we leverage the range of a gradient, a simple, yet robust geometric measures, previously shown to be effective in capturing architectural changes across experimental conditions and species [50–53]. In particular, this metric reflects the spread and differentiation of connectivity profiles across cortical regions along one gradient. In this way, gradient range serves as a proxy for the degree of functional heterogene-

ity: greater ranges indicate more distinct, specialised regions, while reduced ranges signal functional homogenization. The unimodal-to-transmodal gradient range (G1) was preserved across groups compared to the audiovisual (AV) condition, suggesting that the principal gradient remains robust to sensory deprivation (two-tailed T-tests, blind vs. AV: T = -1.93, p = 0.07, FDR BH-corrected, Hedges' g = -0.83; deaf vs. AV: T = 0.27, p = 0.79, FDR BH-corrected, Hedges' g = -0.14; Figure 3B). In contrast, sensory deprivation led to significant contractions in the modality-specific gradients. In blind individuals, the range along the visual gradient (G2) was significantly reduced relative to both audiovisual and auditory conditions (blind vs. AV: T = –4.17, $p < 0.001$, FDR BH-corrected, Hedges' g = –1.78; blind vs. A: T = –2.57, p = 0.02, FDR BH-corrected, Hedges' g = –1.06; AV vs. A: T = 0.86, p = 0.39, FDR BH-corrected, Hedges' g = 0.38). Similarly, a significant reduction in the range of the auditory gradient (G3) was observed exclusively in the deaf group, relative to the typically developed participants exposed to the video-only condition (deaf vs. AV: T = –5.6, $p < 0.001$, FDR BH-corrected, Hedges' g = –2.31; deaf vs. V: T = –3.02, p = 0.01, FDR BH-corrected, Hedges' g = –1.19; AV vs. V: T = 0.71, p = 0.48, FDR BH-corrected, Hedges' g = 0.23). Altogether, these findings suggest that, while not mandatory for the emergence of macroscale gradient architecture, sensory experience plays a critical role in refining the functional differentiation of modality-specific systems. While the hierarchical organization of cortical gradients is preserved in congenital sensory deprivation, unimodal naturalistic stimulation reveals selective reductions in functional heterogeneity along the gradient corresponding to the deprived modality. This observation points to reduced differentiation in sensory-deprived areas, potentially rendering them more responsive to postnatal, experience-driven reorganization.

Functional Reorganization Driven by Sensory Gradients

To further explore the basis of gradient alterations under sensory deprivation, we analysed whole-brain functional connectivity patterns to assess how cortical interactions are reorganised. Treating functional connectivity (FC) matrices as undirected networks, we used the Network-Based Statistic (NBS; [54]) to identify significant differences in edge strength between groups (F=9, $p < 0.05$). For the blind group, FC matrices were compared to those of sighted individuals exposed to audiovisual and auditory-only movies. For the deaf group, comparisons were made against sighted participants exposed to audiovisual and visual-only conditions. This comparison scheme enabled us to isolate changes uniquely associated with congenital sensory deprivation rather than transient differences in unimodal stimulation. A composite null hypothesis test was applied to isolate differences shared across conditions (Figure 4A)[55]. Results showed that reorganisation in both groups primarily involved enhanced connectivity between unimodal and transmodal areas, rather than diffuse connectivity changes. (i.e., greater Pearson correlation between their BOLD timecourses) (see Figure 4A). These effects were consistently more prominent in blind individuals (1% of statistically significant connections altered) than in deaf individuals (0.001% altered).

This approach revealed that congenitally blind individuals exhibit increased connectivity between deprived extrastriate visual areas (e.g., MT+ complex and dorsal stream cortices) and the dorsolateral and inferior frontal cortices (frontoparietal and DMN regions), alongside decrease in intra-visual network connectivity. Congenitally deaf participants showed increased functional coupling between extrastriate visual areas (including the MT+ complex and neighbouring regions) and auditory association cortices (e.g., the superior temporal sulcus and higher-order auditory areas A4 and A5), alongside decreased connectivity within extrastriate visual areas (medial and lateral temporal cortices) and from these regions to medial frontal areas and to subcortical structures (see Supplementary Figure S3 for a version of Figure 4A with the macro-anatomical regions defined by Glasser *et al.* [7]).

Recent work indicates that intrinsic activity and connectivity mature along a hierarchical sensorimotor–association axis, with unimodal and transmodal regions developing along distinct trajectories. In turn, this suggests that such an intrinsic hierarchy may shape processes of experience-dependent functional reorganization [56, 57]. Following this hypothesis and having first shown that individuals with congenital blindness and deafness exhibit a contraction of the gradients corresponding to the deprived sensory modality, we now investigate whether the observed experience-dependent reorganization in functional connectivity is somehow 'constrained' and unfolds along the intrinsic sensory gradients themselves.

We correlated statistical maps of FC differences with the corresponding sensory gradients computed in the typically developed audiovisual group. Thus, checking the correlation between the average involvement of brain areas in the interactions elicited by the sensory deprivation and their position along the corresponding sensory gradient (i.e., the second one for the blind population, the third one for the deaf population) computed on the typically developed audio-video population (Figure 4B). Strikingly, for both blind and deaf individuals, significant positive correlations were observed between the spatial pattern of reorganisation and the corresponding sensory gradient, even after correction for spatial autocorrelation (blind - visual gradient; Spearman rho = 0.42, $p < 0.001$, $p_{null} < 0.001$; deaf - auditory gradient; Spearman rho = 0.36, $p < 0.001$, $p_{null} = 0.003$). This suggests that compensatory connectivity changes in congenitally deprived unimodal cortices unfold along pre-

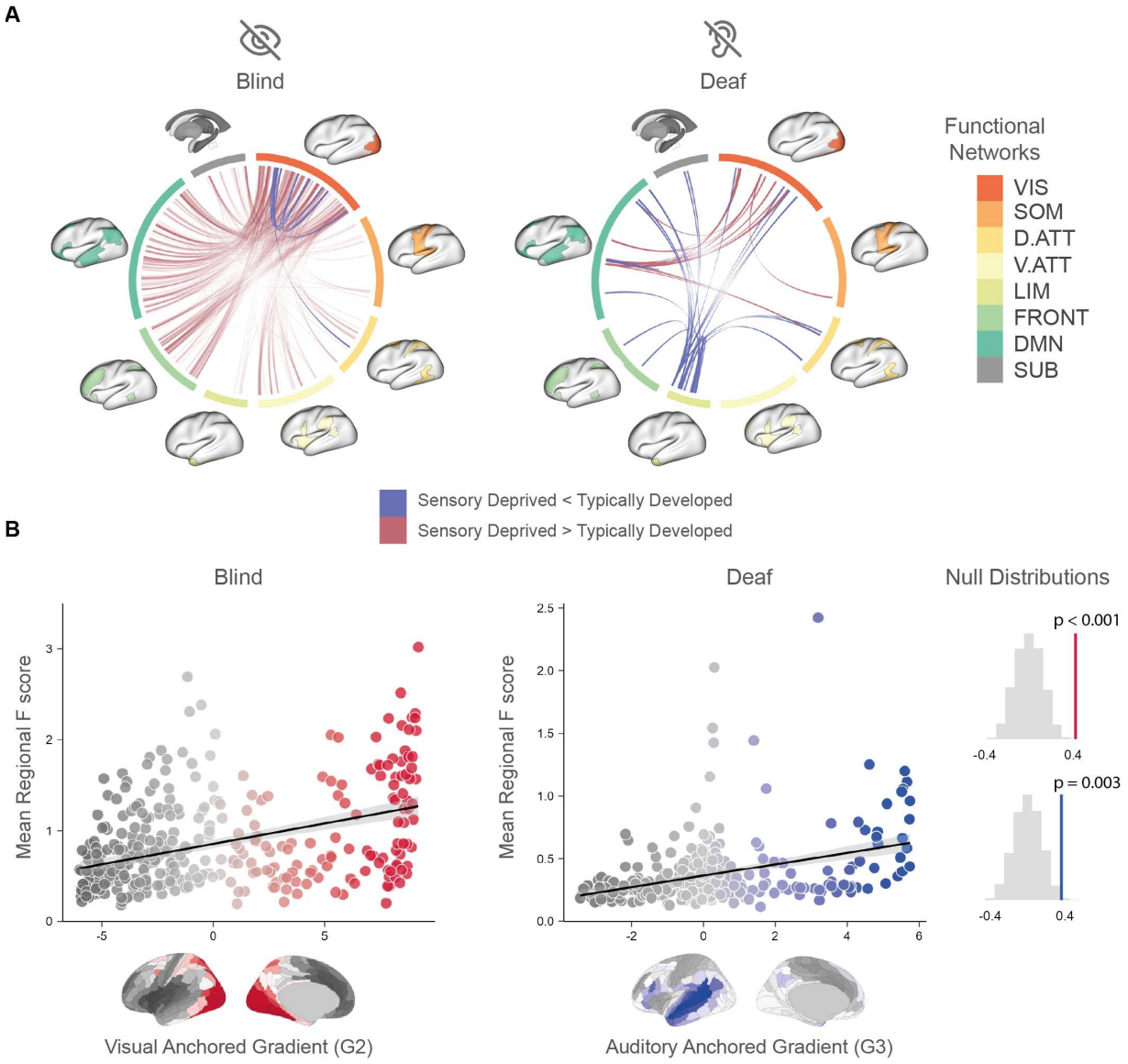

Figure 4. **Functional reconfiguration follows intrinsic cortical hierarchies. A,** Group-level differences in whole-brain functional connectivity between congenitally blind or deaf individuals and matched typically developed controls were identified using the Network-Based Statistic (NBS; $F \geq 9$, $p < 0.05$). Chord diagrams illustrate significantly increased (blue) and decreased (red) connections in each sensory-deprived group. Cortical nodes are grouped by canonical functional networks [58]: VIS = visual, SOM = somatomotor, D.ATT = dorsal attention, V.ATT = ventral attention, LIM = limbic, FRONT = frontoparietal, DMN = default mode, SUB = subcortical. **B,** Mean regional F scores from the NBS analysis were correlated with the spatial layout of the visual-anchored gradient (G2) in the blind group and the auditory-anchored gradient (G3) in the deaf group. Significant positive correlations were observed in both groups, even after correcting for spatial autocorrelation using null distributions derived from 10,000 spatially-constrained surrogate maps ($p < 0.001$ and p = 0.003, respectively; right panel)(Markello and Misic [59], Burt *et al.* [60]; see Methods). This analysis demonstrates that functional reorganization in sensory deprivation unfolds along pre-existing cortical gradients.

existing functional gradients. Of note, this observation favors that intrinsic functional architecture preserves not only large-scale portions of cortical organization, but also 'chaperons' experience-dependent reorganization. To understand the functional relevance of these reorganised networks, we next examined how BOLD activity in regions showing increased FC relates to perceptual content. We correlated BOLD time courses with annotated features of the movie stimulus, ranging from low-level visual (e.g., static Gabor-like filters and motion energy from spatiotemporal integration) and auditory features (e.g., spectral profiles and amplitude envelopes), to mid-level speech-related attributes (e.g., word and letter counts, dialogue presence) and higher-level semantic content (e.g.,

categories of natural vs. artificial elements in auditory and visual streams, and word embeddings derived from subtitles)(Figure 5A)[39]. We then tested for group differences in these correlations to determine whether reorganised regions process distinct content. Results revealed significant group differences in correlations between distinct movie features and activity within regions previously identified as exhibiting increased functional connectivity. Specifically, congenitally deaf participants showed stronger correlations between auditory association cortices and visual movie features compared to the AV control group (deaf vs. AV, two-tailed T-tests, FDR BH-corrected; Left A5, T=5.246, $p = 0.028$, Hedges' g = 2.370; Right A5, T=5.153, $p = 0.033$, Hedges' g = 2.328), while blind individuals showed stronger correlations between deprived visual areas and mid-level speech features compared to AV controls (blind vs. AV, two-tailed T-tests, FDR BH-corrected; Left MT, T=4.937, $p = 0.043$, Hedges' g = 2.167; Left V4t, T=4.918, $p = 0.045$, Hedges' g = 2.158; Right V4, T=5.206, $p = 0.02$, Hedges' g = 2.285; Right LO2, T=5.003, $p = 0.038$, Hedges' g = 2.195; Right V4t, T=6.615, $p = 0.001$, Hedges' g = 2.903; Right FST, T=6.615, $p = 0.009$, Hedges' g = 2.496)(see Figure 5B and Supplementary Figure S4). Thus, we confirm that auditory and speech-related features are redirected to deprived visual cortices in blind individuals, while visual features are rerouted to deprived auditory cortices in deaf individuals, reflecting structured, modality-specific cross-modal reorganization. Altogether, these findings demonstrate that functional reorganization after congenital sensory deprivation adheres to intrinsic cortical hierarchies and supports structured cross-modal processing. Deprived sensory areas do not become functionally dormant; rather, they are recruited for computationally relevant roles through experience-dependent reconfiguration constrained by the brain's inherent architecture.

Robustness and Sensitivity

To assess robustness to the choice of free parameters—specifically the sparsity and diffusion parameters used to compute the functional gradients—the main analysis was replicated across α values of 0.3, 0.7, and 0.9 (see Supplementary Figures S5,S6,S7) and sparsity levels of 70% and 80% (see Supplementary Figures S8,S9). We further evaluated the sensitivity of the NBS findings to a stricter F-threshold ($F = 12$)(see Supplementary Figure S10), confirming the stability of our results. The analysis was then repeated using an alternative parcellation, namely the 400-region functional atlas of Schaefer *et al.* [61], which yielded coherent results preserving the number of relevant interactions (see Supplementary Figure S11). Finally, the stability of the feature-correlation analysis was assessed by replacing word counts with a binary indicator of dialogue presence in each TR (see Supplementary Figure S12).

DISCUSSION

How do sensory experience and innate organisational principles jointly shape the macroscale functional architecture of the cortex? Here, leveraging naturalistic stimulation and functional gradient analyses, we compare three distinct sensory conditions—audiovisual, visual-only, and auditory-only— in congenitally blind, congenitally deaf, and neurotypically developed individuals to examine whether sensory deprivation affects hierarchies and functional gradients.

We demonstrate that congenital sensory deprivation does not disrupt the overall hierarchical organization of cortical functional gradients. However, sensory-deprived cortices exhibit reduced functional differentiation, in particular along the gradient dimension associated with the deprived modality. This reduced differentiation appears to facilitate postnatal, experience-dependent modelling of deprived cortical areas. Notably, such reorganization unfolds along the intrinsic sensory gradients themselves, with perceptual information from spared unimodal or transmodal regions being systematically rerouted to sensory-deprived areas. Altogether, these results underscore that the development of cortical architecture emerges from a dynamic interplay between intrinsic, genetically driven organizational frameworks and extrinsic, experience-dependent shaping forces.

Brain macroscale functional organization appears both to be anchored by innate hierarchies that constrain plasticity, yet sufficiently flexible to accommodate profound changes in sensory experience from the earliest stages of development. Extending recent observations by Samara *et al.* [44], our data indicate that during naturalistic processing, the primary gradient retains its canonical resting-state configuration, spanning from unimodal sensory to transmodal regions, independent of sensory experience.

This robust preservation aligns with evolutionary and developmental evidence that suggest an intrinsic organisational scaffold underpinning large-scale functional architecture [27]. Indeed, prior studies support the notion that the principal gradient may reflect fundamental organising principles anchored by intrinsic factors, such as gene expression patterns and cortical microstructure, transcending specific sensory modalities [12, 39, 40, 62–66].

In contrast, we observed selective alterations in the geometric properties (i.e., contractions in the gradient range) of the secondary gradients corresponding to deprived sensory modalities. Gradient range has previously been established as a sensitive biomarker of functional heterogeneity across the cortical surface, with broader ranges denoting greater differentiation, and narrower ranges reflecting more homogeneous functional architectures [50–53].

In the context of congenital deprivation, reduced range in visual or auditory gradients likely reflects a disruption of this maturational refinement process, whereby

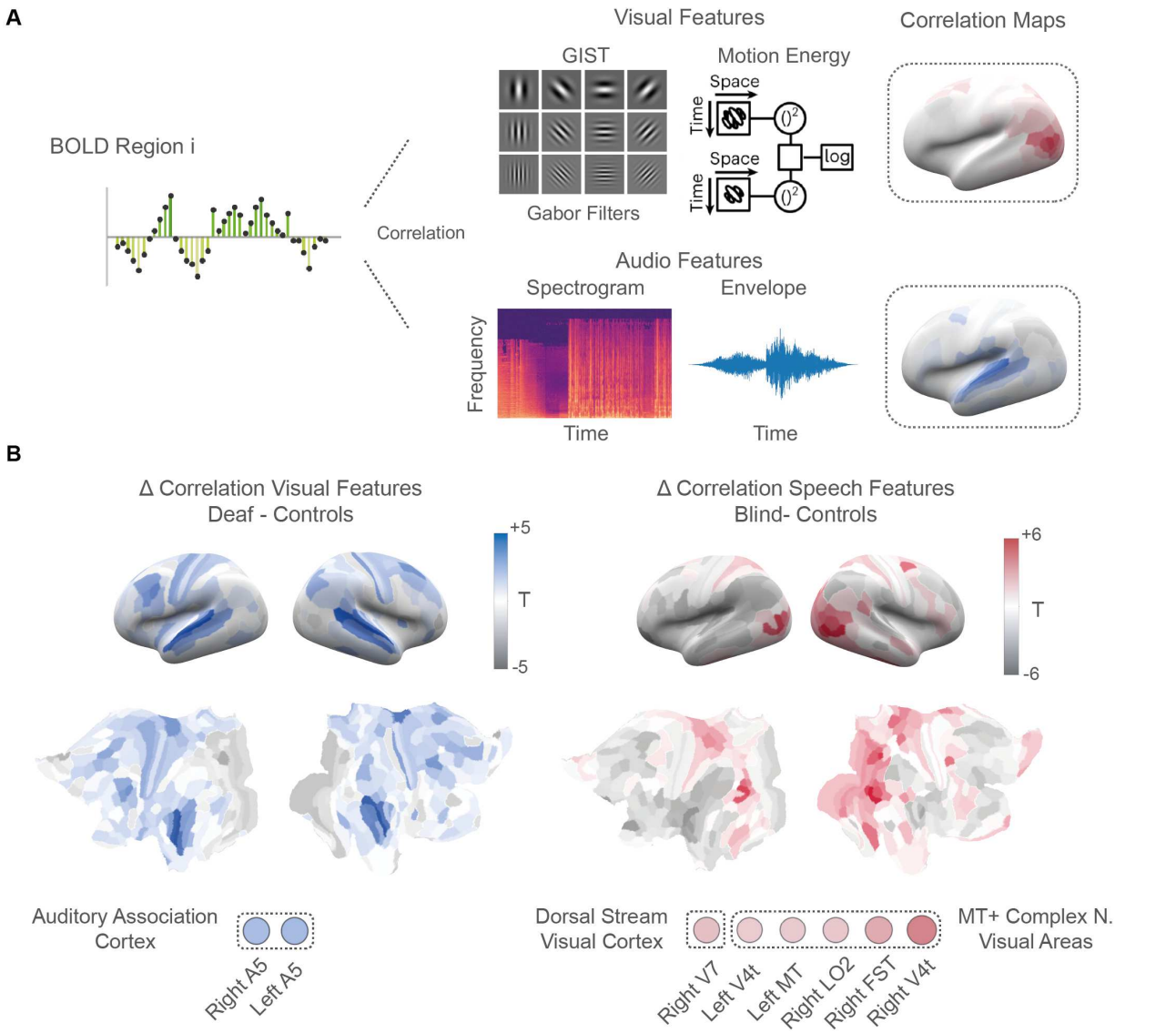

Figure 5. **Feature-specific recruitment of deprived sensory cortices. A,** Schematic of the analytical pipeline: BOLD time series from each cortical region were correlated with time courses of annotated stimulus features, including low-level visual (e.g., Gabor filters, motion energy), low- and mid-level auditory features (e.g., spectrogram, envelope), and speech-related semantic features. Correlation maps were generated per subject and compared across groups **B,** Surface renderings and inflated ROI maps show results from region-wise two-tailed t-tests contrasting sensory-deprived and typically developed individuals. Left: Deaf participants exhibit significantly stronger correlations between visual stimulus features and auditory association cortices (blue, $p < 0.05$ FDR BH-corrected). Right: Blind participants show significantly stronger correlations between speech-related features and visual cortices, including MT+ and dorsal stream regions (red, $p < 0.05$ FDR BH-corrected). Insets highlight significant clusters and annotated ROIs.

modality-specific input is typically required to sculpt the fine-grained functional topography of unimodal areas. Importantly, this reduction is not global but modality-specific, selectively affecting the gradient dimension anchored in the deprived sensory cortex. The modality-specific nature of this gradient contraction highlights their sensitivity as indicators of experience-driven differentiation.

Our findings support a dual-mechanism model wherein intrinsic, genetically guided structural constraints establish a stable global hierarchical scaffold, while sensory experience fine-tunes local cortical specialisation [16, 25, 43, 52]. This dual influence of structural anchoring and sensory-driven refinement closely aligns with recent theoretical models suggesting that functional specialization is not solely dictated by sensory input, but also by the computational goals of each cortical area, its embeddedness in pre-existing anatomical and functional networks and experience-dependent adaptation [10, 37–39, 67, 68].

Our gradient-based findings are complemented by finer-grained connectivity analyses revealing modality-specific reorganization patterns. Previous evidence showed modified functional connectivity between deprived unimodal cortices and non-deprived unimodal or transmodal areas during sensory processing (e.g., Amaral *et al.* [62], Anurova *et al.* [69], Bauer *et al.* [70], Amaral *et al.* [71]). Consistently, in congenitally blind individuals, we observe increased connectivity between extrastriate and key hubs of the frontoparietal and default mode networks.

This increased visual-to-frontal integration occurs alongside a reduction in intra-network connectivity within the visual system itself, suggesting a reorganization of functional resources toward higher-order transmodal regions. Additionally, the emergent connectivity between the deprived visual cortex and the default mode network in blind individuals mirrors the functional reorganization observed in sensorimotor cortex after limb loss, suggesting that, in the absence of primary input, cortical regions may be reallocated to internally driven functions through integration with transmodal networks [72].

A complementary pattern emerges in congenitally deaf individuals, who exhibited strengthened connectivity between the visual network and auditory association cortices, notably the superior temporal sulcus and high-level auditory regions. Therefore, our findings confirm that deprived unimodal cortices develop reorganized, structured interactions with functionally and topographically distant regions. By testing the relationship between the spatial distribution of functional changes and the underlying sensory hierarchy, we also showed that this functional reorganization follows the pre-existing sensory hierarchies of the brain. In other words, deprived cortical regions tend to establish new connections with areas that already lie along specific functional gradients, reflecting the typical sensory organization.

This implies that the brain's intrinsic architecture not only remains intact in the absence of sensory input, but also actively 'chaperons' plastic reorganization along inherent large-scale structure. Consequently, the altered connectivity patterns in blind and deaf people provide compelling support for the idea that functional reorganization unfolds along meaningful computational and anatomical trajectories, and highlight how intrinsic geometry and long-range pathways enable the deprived sensory cortex not only to remain functionally relevant but to contribute adaptively to non-canonical information processing through experience-dependent reconfiguration.

Importantly, these reorganized interactions appear to reflect specific patterns of feature-oriented integration of perceptual information on low/mid-level features. Our data also reveal a distinctive pattern of functional recruitment that differs fundamentally between blindness and deafness, pointing to important differences in the reorganizational potential of the occipital and temporal cortices. The occipital cortex's extensive intrinsic and extrinsic connections, early maturation, and central hierarchical positioning confer exceptional versatility and computational flexibility, facilitating significant functional repurposing in blind individuals [12, 38, 73, 74]. In contrast, the auditory cortex demonstrates relatively constrained reorganizational potential, relying primarily on strengthening pre-existing heteromodal connections modulated by top-down influences from transmodal regions [75].

In the light of our results, we propose that intrinsic architectural functional geometry governs spatially extended cross-modal plasticity, thus providing a unified model explaining both stability and flexibility in sensory-deprived brains. Explicitly testing the evolution of chronic readjustment, longitudinal studies across different developmental stages (including late-onset sensory deprivation) will be invaluable to determine whether functional changes occur within a critical period or persist beyond it. Recent evidence from congenitally sensory-deprived individuals shows that meaningful, content-specific representations can emerge independently of a postnatal experience, pointing to an organizational blueprint or proto-architecture that predates and scaffolds experience-dependent specialization (e.g., Ricciardi and Pietrini [12], Ricciardi *et al.* [38], Setti *et al.* [39], Arcaro and Livingstone [67]). Notably, supramodal processing — where cortical regions encode conceptual content regardless of sensory modality — has been extensively demonstrated and supports the idea of modality-independent representational formats across sensorimotor experiences and higher cognitive functioning [12, 38].

Moreover, this perspective aligns with evidence that even primary sensory areas, traditionally viewed as unimodal, are embedded in a richly interconnected architecture that supports early multisensory integration. Unimodal cortices may exhibit the capacity to integrate cross-modal input that becomes functionally dominant when the canonical sensory input is absent, as often seen in sensory deprivation [76, 77]. In addition, our data could also be integrated into the framework arguing that the brain's functional architecture is structured to encode and respond to features of sensory experience that transcend any single modality.

In this view, the dialogue across modalities, rather than a mere compensatory adaptation, reflects an intrinsic, supramodal infrastructure that allows the brain to flexibly route, compare, and integrate inputs from different sensory systems to detect and respond to environmentally relevant changes (e.g., Novembre and Iannetti [78]).

In summary, our study highlights that the macroscale functional architecture of the cortex emerges from a dynamic interplay between genetically guided intrinsic constraints and extrinsic sensory experience. Functional gradients provide a valuable framework to understand this dual influence, illustrating how innate structural scaffolds impose consistent organisational principles while remain-

ing sufficiently plastic to accommodate adaptive changes. Our findings demonstrate that even under conditions of extreme sensory input loss, cortical reorganisation remains anchored within existing hierarchical structures, underscoring the presence of a stable cortical blueprint. Brain macroscale functional organisation appears both to be anchored by innate hierarchies that constrain plasticity, yet sufficiently flexible to accommodate profound changes in sensory experience from the earliest stages of development.

MATERIALS AND METHODS

Ethical statement

We took advantage of a previously acquired dataset, and full details are provided in the original publication [39]. Each volunteer was instructed about the nature of the research and gave written informed consent for participation, in accordance with the guidelines of the institutional board of the Turin University, Brain Imaging Centre. The study was approved by the Ethical Committee of the University of Turin (protocol number 195874, May 29th 2019) and conforms to the Declaration of Helsinki. Data used in this analysis were drawn from the study by Setti *et al.* [39], meaning the participant sample, stimulation, data acquisition and preprocessing is identical to the one described in the original work, as outlined in the following paragraphs.

Participants

Fifty participants took part in the study. As already documented in Setti *et al.* [39], thirty normally-developed (TD) individuals and twenty sensory-deprived (SD) subjects (born without visual or auditory experience) were enrolled. The TD group was split into three equal samples, each exposed to one version of the same feature film: (1) full audiovisual (AV), $N = 10$ (age 35 ± 13yr; 8 females), (2) auditory only (A), $N = 10$ (age 39 ± 17yr; 7 females), (3) visual only (V), $N = 10$ (age 37 ± 15yr; 5 females). The SD cohort comprised congenitally blind participants ($N = 11$, mean age 46 ± 14yr; 3 females) who viewed the A version, and congenitally deaf participants ($N = 9$, mean age 24 ± 4yr; 5 females) who viewed the V version. Two blind subjects were excluded from the fMRI analyses due to excessive head motion (final SD sample: $N = 9$, mean age 44 ± 14yr; 3 females). All participants were right-handed according to the Edinburgh Handedness Inventory, native Italian speakers, and had no history of neurological or psychiatric disorders. The deaf group was proficient in Italian Sign Language and did not use hearing aids; the TD group reported normal or corrected-to-normal vision, intact hearing, and no knowledge of sign language. Further details for the SD participants are provided in Supplementary Materials of Setti *et al.* [39].

Naturalistic stimulus

Following Setti *et al.* [39], naturalistic stimulation was provided via three versions—visual (V), auditory (A) and audiovisual (AV)—of the live-action film *101 Dalmatians* (Herek, Great Oaks Entertainment & Walt Disney, 1996). To facilitate compliance during unimodal presentation, a linear-plot narrative was selected. The original film was edited to fit a single scanning session by omitting non-essential scenes and splicing remaining footage to maintain narrative continuity. The final cut spans approximately 54 minutes and is divided into six runs of ∼8 minutes each, each preceded and followed by a 6 s fade-in and fade-out.

For the A condition, an Italian audio description was professionally recorded and overlaid on the film's original soundtrack to convey omitted visual content. The script was adapted to bridge edited gaps and to describe essential visual elements not captured by dialogue or music. Recording was performed in a noise-isolated studio using a Neumann U87 ai microphone, Universal Audio LA 610 mk2 preamplifier, Apogee Rosetta converter, and Logic Pro 10.4. The voice track was then mixed with the original audio, and fade effects were applied to smooth transitions between runs; music and narration were subsequently remixed for level balance.

The complete soundscape (dialogue, narration, environmental sounds) was transcribed into style- and color-coded subtitles to distinguish speaking voices and aid comprehension. Line breaks were adjusted (one- or two-line formats) to avoid interference with reading or visual processing. Video editing was carried out in iMovie (v10.1.10), and subtitles were authored using Aegisub (v3.2.2, http://www.aegisub.org/). In the V and AV conditions, a small red fixation cross was superimposed at screen center, with subtitles displayed at the bottom.

fMRI experimental design

Prior to scanning, all participants rated their familiarity with the film's plot on a 5-point Likert scale (1 = not at all, 5 = very well). During fMRI acquisition, each experimental subgroup viewed one of the edited versions of the film (V, A or AV) and were instructed simply to enjoy the presentation. Structural and functional MRI data were collected in a single session. Upon completion of imaging, engagement and compliance were evaluated using a custom two-alternative forced-choice questionnaire probing key narrative elements.

Stimulation setup

Audio and visual stimuli were presented via MR-compatible LCD goggles and headphones (VisualStim Resonance Technology; video resolution 800×600 at 60Hz; visual field 30°×22°; 5" display; audio attenuation 30dB; frequency response 40Hz–40kHz). Both devices were supplied to all participants regardless of experimental condition. Stimulus delivery was managed using Presentation 16.5 (Neurobehavioral Systems; http://www.neurobs.com).

fMRI data acquisition and preprocessing

Functional MRI data were acquired on a Philips 3T Ingenia scanner equipped with a 32-channel head coil. Gradient-echo EPI sequences were used with the following parameters: TR = 2000 ms; TE = 30 ms; FA = 75°; FOV = 240 mm; matrix = 80×80; slice thickness = 3 mm; voxel size = 3×3×3 mm; 38 axial slices acquired in ascending order; 1614 volumes were collected across the six movie runs, with an additional 256 volumes for the scrambled control run. High-resolution T1-weighted anatomical images were obtained using an MPRAGE sequence (TR=7ms; TE=3.2ms; FA=9°; FOV=224mm; matrix=224×224; slice thickness=1mm; voxel size=1×1×1mm; 156 sagittal slices). Data acquisition and analysis were conducted with full knowledge of experimental conditions.

Preprocessing followed standard AFNI (v17.1.12) workflows. First, spike artifacts were removed (3dDespike), and all volumes within each run were slice-time corrected (3dTshift) and realigned to the first volume of the first run (3dvolreg). Spatial smoothing was applied using a 6mm FWHM Gaussian kernel (3dBlurToFWHM), followed by percent signal normalization. Each run was detrended using a Savitzky–Golay filter (polynomial order=3, frame length=200 timepoints) in MATLAB R2019b to remove low-frequency drifts and outliers. The runs were then concatenated, and nuisance regressors—including motion parameters and spike regressors for framewise displacements > 0.3mm—were removed via multiple regression (3dDeconvolve). Band-pass temporal filtering was implemented retaining frequencies between 0.008 and 0.08 Hz. Finally, individual participant time series were nonlinearly warped to MNI-192 standard space using 3dQWarp.

Movie annotations

In the previous work by Setti *et al.* [39], the authors derived a set of movie-related features by means of computational modeling. Among these, low-level features were characterized both for the auditory and visual streams, thus capturing spectral (frequency) and sound envelope properties on one hand and static Gabor-like filters (GIST) and motion energy information on the other. Additionally, high-level features were defined based on manually tagged natural and artificial categories as well as word embeddings from subtitles. For the latter, two alternative embeddings were developed: one from individual sentences, utilizing the pretrained English-based GPT-3 model to fully capture semantic compositionality, and one using single-word embeddings generated with the Word2Vec algorithm trained on an Italian corpus. This produced two high-level semantic models, one combining categorical data with GPT-3 embeddings and the other with Word2Vec embeddings. Features related to the film's editing were also annotated (such as scene transitions, cuts, dialogues, music, and audio descriptions). To remove shared variance across models, each stimulus model was orthogonalized with respect to movie editing descriptors. The editing features (e.g., cuts, transitions, dialogues, and music) were shown to influence both low-level descriptors (e.g., shifts in visual and auditory properties at scene transitions) and high-level semantic descriptors (e.g., spoken and written dialogues), potentially masking the finer computational features and inflating the explained variance. The methodological approach and results are detailed in Supplementary Information of the original work. Based on the movie script, two new speech-specific annotations were created. The script was segmented according to the repetition time (TR) of the functional images, with each time window annotated to indicate the binary presence or absence of dialogue. Additionally, a letter count within each segment was included to model the presence of human speech at a low level of complexity.

Brain Parcellations

Cortical segmentation was performed using the 360-region multimodal parcellation of Glasser *et al.* [7], which provides functional and anatomical cortical mapping. Exclusively for analyses not concerning cortical gradients (i.e., Fig.4A and Fig.5), the dataset was complemented by 32 subcortical ROIs from the work of Tian *et al.* [79]. Within each ROI, denoised BOLD-signal time series were averaged across all voxels to yield a single representative time course. These ROI-wise time courses were then extracted for subsequent analyses. One participant in the deaf cohort was excluded because the R_TGv region lay almost entirely outside the acquired volume.

Analytical Pipeline

Functional gradients from diffusion map embedding

Cortical functional gradients were calculated using the BrainSpace toolbox (https://github.com/MICA-MNI/BrainSpace) in Python, applying default settings

for kernel sparsity estimation (0.9), similarity kernel (cosine similarity), and anisotropic diffusion parameter (α=0.5). We calculated the functional connectivity matrix (FC) computing for each ROI s of the HCP Atlas [7] the Pearson correlation with all the other cortical areas. The obtained matrix was then row-wise z-transformed and thresholded to obtain a 10% density, thus retaining only the strongest interactions and removing possible spurious effects. Given the resultant matrix, a normalized cosine angle affinity matrix is computed, indicating the similarity in connectivity patterns for each pair of ROIs. Finally, the obtained affinity matrix is embedded in a low-dimensional space by means of diffusion map embedding. This approach has the advantage, compared to other approaches like PCA, of being nonlinear and thus it allows to account for more complex patterns. The algorithm is governed by parameters α and t, where α determines the influence of the density of sampling points on the manifold ($\alpha = 0$ indicates maximal influence, while $\alpha = 1$ indicates none) and it adjusts the scale of eigenvalues in the diffusion operator. Following previous recommendations, we set α to 0.5 and t to 0 to maintain global relationships between data points in the embedded space. Setting t = 0 allows the diffusion time to be automatically estimated via a damped regularization process. Then, Procrustes rotation was used to align the obtained gradients to the average gradient of the typically-developed subjects exposed to the audiovisual stimulation. This procedure corrects for potential ambiguities in eigenvector ordering (such as sign flipping or changes in explained variance), ensuring that gradients computed separately for each individual are directly comparable and therefore improving the stability of the results. In order to assess whether the heterogeneity expressed along each gradient was altered we computed the numerical range of each of the first three gradient as the difference between the minimum and maximum eigenvector values. This metric reflects the degree of segregation, or in other words the distinct connectivity profiles, between the gradient extremes.

Network Based Statistic

To determine the statistically significant difference in FC between distinct groups we employed a network-based statistical approach. This nonparametric statistical method controls family-wise error rates in network data by accounting for multiple comparisons. It first identifies connected components within the graph, based on edges that are significantly above the statistical threshold (F-contrast; here, an F-value threshold of 9, two-sided, with an alpha level of 0.05). The statistical significance of each connected component is then assessed by comparing its topology to a null distribution derived from nonparametric permutation testing of component sizes. By testing on a component-by-component basis, this approach achieves greater statistical power compared to mass-univariate methods. Our aim was to identify consistent changes across multiple comparisons excluding effects related to the temporary absence of a sensory modality. Following the approach by Luppi *et al.* [55], we employed a composite null hypothesis significance test, where the null hypothesis assumes that at least one of the datasets has no effect. Rejecting the null hypothesis requires that all comparisons show non-zero effects. This test compares an observed test statistic to a null distribution, with the test statistic defined as the minimum of the three F-scores from the relevant comparisons (e.g., audio video vs. blind, blind vs. audio, but not audio video vs. audio). To construct the null distribution, we performed 500 iterations of selective label reshuffling. In each iteration, we randomly permuted the labels of a single comparison and recalculated the F-scores. By altering only one comparison at a time—rather than permuting all labels simultaneously—this procedure evaluates the observed data against the "least altered" configuration compatible with the null hypothesis. This method represents a least favorable configuration test, ensuring control over the false positive rate below a threshold of 0.05.

Brain correlation with film annotations

To establish how each ROI correlates with the audio, video, semantic, and speech movie features for each ROI in the cortical atlas, the Pearson correlation was computed between the corresponding BOLD signal and the features timeseries. When more than one feature was present for a given category, the maximum observed correlation was considered. With respect to the speech time series, to account for possible dependencies with the low-level auditory features, analyses were performed using partial Pearson correlation, regressing out the effects attributable to the low level sound properties, and thus retaining the correlation between the residuals and the BOLD signal. The statistical significance was FDR corrected for all tests performed.

Statistical reporting

The correlation between functional gradients was evaluated using Spearman's rank-based, non-parametric correlation coefficient to ensure robustness against outliers. To mitigate potential biases from spatial autocorrelation, we computed corrected p-values using an autocorrelation-preserving null model [60]. We simulated surrogate brain maps with spatial autocorrelation that matched the one of the original brain maps of interest that is functional gradients and movie parcellation. Using the geodetic distance matrix from the atlas as input, we generated 10,000 surrogate maps that preserve spatial autocorrelation. We then computed Spearman's rank-based correlation for each of the obtained maps. The nonparametric p-values were computed considering the

number of the correlation with surrogate maps that exceeded the observed correlation with the original data. For group comparisons, two-sample t-tests with Welch's correction [80] were applied to account for unequal variances. Correction for multiple comparisons was carried out using the Benjamini-Hochberg False Discovery Rate correction [81], with significance set at an alpha level of 0.05. Effect sizes were reported using Hedges's g [82], a standardized measure that provides a less biased estimate of mean difference and that is especially useful for small sample sizes.

Contributions

D.O., F.S., A.I.L. and E.R conceived and developed the study idea; F.S., and E.R. designed the experiments; F.S. collected the data; D.O and F.S. analysed the data; D.O., F.S., A.I.L. and E.R wrote the original draft with valuable revisions by M.T, G.P. and M.P. All authors contributed to review and editing. G.P., M.T., A.I.L. and E.R., supervised the project. All authors approved the manuscript.

Acknowledgments

We would like to thank all the people behind the *101 Dalmatians* project. We thank Daniel Margulies, Marcin A. Radecki, Luca Cecchetti, Davide Bottari, Giacomo Handjaras and the colleagues for suggestions on the research project and data processing.

A.I.L. acknowledges support from St John's College, Cambridge; and a Wellcome Early Career Award (grant number 226924/Z/23/Z).

G.P. acknowledges partial support by ERC Consolidator Grant RUNES (Grant no. 101171380) and the MSCA Doctoral Network *BeyondTheEdge* (Grant no. 101120085).

M.T. is supported by PRIN 2022 (2022NEE53Z) from the Ministry of University and Research (MUR), the National Recovery and Resilience Plan – PNRR – "MNESYS" (PE00000006), with a specific contribution from the sub-project ("bando a cascata") "SPARKS" (CUP D93C22000930002), and the ERC Proof of Concept "PRISM" (1011583).

E.R. work was supported by the PRIN grants (20223K8B3X and P20228PHN2) by the Italian Ministry of University and Research and by the "Tuscany Health Ecosystem—THE" Project, Spoke 8, granted by Next Generation EU—National Recovery and Resilience Plan (Piano Nazionale di Ripresa e Resilienza, NRRP)—Mission 4 Component 2 Investment 1.4—Ministry of University and Research (MUR) Call N. 3277, Project Code ECS00000017 to E.R.

Conflicts of interest

The authors have no conflicts of interest to declare.

[1] P. Rakic, "Specification of Cerebral Cortical Areas," Science **241**, 170–176 (1988).

[2] D. D. O'Leary, S.-J. Chou, and S. Sahara, "Area Patterning of the Mammalian Cortex," Neuron **56**, 252–269 (2007).

[3] D. H. Hubel and T. N. Wiesel, "BINOCULAR INTERACTION IN STRIATE CORTEX OF KITTENS REARED WITH ARTIFICIAL SQUINT," Journal of Neurophysiology **28**, 1041–1059 (1965).

[4] W. T. Greenough, J. E. Black, and C. S. Wallace, "Experience and Brain Development," Child Development **58**, 539 (1987).

[5] M. H. Johnson, "Functional brain development in humans," Nature Reviews Neuroscience **2**, 475–483 (2001).

[6] D. C. Van Essen and D. L. Dierker, "Surface-Based and Probabilistic Atlases of Primate Cerebral Cortex," Neuron **56**, 209–225 (2007).

[7] M. F. Glasser, T. S. Coalson, E. C. Robinson, C. D. Hacker, J. Harwell, E. Yacoub, K. Ugurbil, J. Andersson, C. F. Beckmann, M. Jenkinson, S. M. Smith, and D. C. Van Essen, "A multi-modal parcellation of human cerebral cortex," Nature **536**, 171–178 (2016).

[8] D. Maurer, T. Lewis, and C. Mondloch, "Missing sights: consequences for visual cognitive development," Trends in Cognitive Sciences **9**, 144–151 (2005).

[9] A. Pascual-Leone, A. Amedi, F. Fregni, and L. B. Merabet, "THE PLASTIC HUMAN BRAIN CORTEX," Annual Review of Neuroscience **28**, 377–401 (2005).

[10] I. Fine and J.-M. Park, "Blindness and Human Brain Plasticity," Annual Review of Vision Science **4**, 337–356 (2018).

[11] D. Bavelier and H. J. Neville, "Cross-modal plasticity: where and how?" Nature Reviews Neuroscience **3**, 443–452 (2002).

[12] E. Ricciardi and P. Pietrini, "The supramodality "spillover" from neuroscience to cognitive sciences: a commentary on Calzavarini (2024)," Language, Cognition and Neuroscience **39**, 867–871 (2024).

[13] B. R. Payne and S. G. Lomber, "Reconstructing functional systems after lesions of cerebral cortex," Nature Reviews Neuroscience **2**, 911–919 (2001).

[14] E. Bullmore and O. Sporns, "The economy of brain network organization," Nature Reviews Neuroscience **13**, 336–349 (2012).

[15] A. R. McIntosh, "Contexts and Catalysts: A Resolution of the Localization and Integration of Function in the Brain," Neuroinformatics **2**, 175–182 (2004).

[16] A. I. Luppi, F. E. Rosas, P. A. Mediano, A. Demertzi, D. K. Menon, and E. A. Stamatakis, "Unravelling consciousness and brain function through the lens of time, space, and information," Trends in Neurosciences **47**, 551–568 (2024).

[17] R. V. Raut, A. Z. Snyder, and M. E. Raichle, "Hierarchical dynamics as a macroscopic organizing principle of the human brain," Proceedings of the National Academy of Sciences **117**, 20890–20897 (2020).

[18] J. D. Murray, A. Bernacchia, D. J. Freedman, R. Romo, J. D. Wallis, X. Cai, C. Padoa-Schioppa, T. Pasternak, H. Seo, D. Lee, and X.-J. Wang, "A hierarchy of intrinsic timescales across primate cortex," Nature Neuroscience **17**, 1661–1663 (2014).

[19] M. Mesulam, "From sensation to cognition," Brain **121**, 1013–1052 (1998).

[20] R. L. Buckner and F. M. Krienen, "The evolution of distributed association networks in the human brain," Trends in Cognitive Sciences **17**, 648–665 (2013).

[21] C. Murphy, H.-T. Wang, D. Konu, R. Lowndes, D. S. Margulies, E. Jefferies, and J. Smallwood, "Modes of operation: A topographic neural gradient supporting stimulus dependent and independent cognition," NeuroImage **186**, 487–496 (2019).

[22] M. Mesulam, "The evolving landscape of human cortical connectivity: Facts and inferences," NeuroImage **62**, 2182–2189 (2012).

[23] J. M. Huntenburg, P.-L. Bazin, and D. S. Margulies, "Large-Scale Gradients in Human Cortical Organization," Trends in Cognitive Sciences **22**, 21–31 (2018).

[24] B. Vázquez-Rodríguez, L. E. Suárez, R. D. Markello, G. Shafiei, C. Paquola, P. Hagmann, M. P. Van Den Heuvel, B. C. Bernhardt, R. N. Spreng, and B. Misic, "Gradients of structure–function tethering across neocortex," Proceedings of the National Academy of Sciences **116**, 21219–21227 (2019).

[25] C. C. Hilgetag and A. Goulas, "'Hierarchy' in the organization of brain networks," Philosophical Transactions of the Royal Society B: Biological Sciences **375**, 20190319 (2020).

[26] D. S. Margulies, S. S. Ghosh, A. Goulas, M. Falkiewicz, J. M. Huntenburg, G. Langs, G. Bezgin, S. B. Eickhoff, F. X. Castellanos, M. Petrides, E. Jefferies, and J. Smallwood, "Situating the default-mode network along a principal gradient of macroscale cortical organization," Proceedings of the National Academy of Sciences **113**, 12574–12579 (2016).

[27] V. J. Sydnor, B. Larsen, D. S. Bassett, A. Alexander-Bloch, D. A. Fair, C. Liston, A. P. Mackey, M. P. Milham, A. Pines, D. R. Roalf, J. Seidlitz, T. Xu, A. Raznahan, and T. D. Satterthwaite, "Neurodevelopment of the association cortices: Patterns, mechanisms, and implications for psychopathology," Neuron **109**, 2820–2846 (2021).

[28] C. Paquola, R. Vos De Wael, K. Wagstyl, R. A. I. Bethlehem, S.-J. Hong, J. Seidlitz, E. T. Bullmore, A. C. Evans, B. Misic, D. S. Margulies, J. Smallwood, and B. C. Bernhardt, "Microstructural and functional gradients are increasingly dissociated in transmodal cortices," PLOS Biology **17**, e3000284 (2019).

[29] S. F. Beul and C. C. Hilgetag, "Neuron density fundamentally relates to architecture and connectivity of the primate cerebral cortex," NeuroImage **189**, 777–792 (2019).

[30] L. H. Scholtens, R. Schmidt, M. A. De Reus, and M. P. Van Den Heuvel, "Linking Macroscale Graph Analytical Organization to Microscale Neuroarchitectonics in the Macaque Connectome," The Journal of Neuroscience **34**, 12192–12205 (2014).

[31] F. M. Krienen, B. T. T. Yeo, T. Ge, R. L. Buckner, and C. C. Sherwood, "Transcriptional profiles of supragranular-enriched genes associate with corticocortical network architecture in the human brain," Proceedings of the National Academy of Sciences **113** (2016), 10.1073/pnas.1510903113.

[32] S. Froudist-Walsh, T. Xu, M. Niu, L. Rapan, L. Zhao, D. S. Margulies, K. Zilles, X.-J. Wang, and N. Palomero-Gallagher, "Gradients of neurotransmitter receptor expression in the macaque cortex," Nature Neuroscience **26**, 1281–1294 (2023).

[33] R. Gao, R. L. Van Den Brink, T. Pfeffer, and B. Voytek, "Neuronal timescales are functionally dynamic and shaped by cortical microarchitecture," eLife **9**, e61277 (2020).

[34] C. Honey, T. Thesen, T. Donner, L. Silbert, C. Carlson, O. Devinsky, W. Doyle, N. Rubin, D. Heeger, and U. Hasson, "Slow Cortical Dynamics and the Accumulation of Information over Long Timescales," Neuron **76**, 423–434 (2012).

[35] D. J. Felleman and D. C. Van Essen, "Distributed hierarchical processing in the primate cerebral cortex." Cerebral cortex (New York, NY: 1991) **1**, 1–47 (1991).

[36] A. S. Keller, V. J. Sydnor, A. Pines, D. A. Fair, D. S. Bassett, and T. D. Satterthwaite, "Hierarchical functional system development supports executive function," Trends in Cognitive Sciences **27**, 160–174 (2023).

[37] E. Ricciardi, G. Handjaras, and P. Pietrini, "The blind brain: How (lack of) vision shapes the morphological and functional architecture of the human brain," Experimental Biology and Medicine **239**, 1414–1420 (2014).

[38] E. Ricciardi, D. Bottari, M. Ptito, B. Röder, P. Pietrini, *et al.*, "The sensory-deprived brain as a unique tool to understand brain development and function," Neuroscience and biobehavioral reviews **108**, 78–82 (2020).

[39] F. Setti, G. Handjaras, D. Bottari, A. Leo, M. Diano, V. Bruno, C. Tinti, L. Cecchetti, F. Garbarini, P. Pietrini, and E. Ricciardi, "A modality-independent proto-organization of human multisensory areas," Nature Human Behaviour **7**, 397–410 (2023).

[40] G. Lettieri, G. Handjaras, E. M. Cappello, F. Setti, D. Bottari, V. Bruno, M. Diano, A. Leo, C. Tinti, F. Garbarini, P. Pietrini, E. Ricciardi, and L. Cecchetti, "Dissecting abstract, modality-specific and experience-dependent coding of affect in the human brain," Science Advances **10**, eadk6840 (2024).

[41] C. González-García and B. J. He, "A Gradient of Sharpening Effects by Perceptual Prior across the Human Cortical Hierarchy," The Journal of Neuroscience **41**, 167–178 (2021).

[42] R. Hardstone, M. Zhu, A. Flinker, L. Melloni, S. Devore, D. Friedman, P. Dugan, W. K. Doyle, O. Devinsky, and B. J. He, "Long-term priors influence visual perception through recruitment of long-range feedback," Nature Communications **12**, 6288 (2021).

[43] T. H. Murphy and D. Corbett, "Plasticity during stroke recovery: from synapse to behaviour," Nature Reviews

Neuroscience **10**, 861–872 (2009).
[44] A. Samara, J. Eilbott, D. S. Margulies, T. Xu, and T. Vanderwal, "Cortical gradients during naturalistic processing are hierarchical and modality-specific," NeuroImage **271**, 120023 (2023).
[45] U. Hasson, Y. Nir, I. Levy, G. Fuhrmann, and R. Malach, "Intersubject synchronization of cortical activity during natural vision," science **303**, 1634–1640 (2004).
[46] R. R. Coifman and S. Lafon, "Diffusion maps," Applied and Computational Harmonic Analysis **21**, 5–30 (2006).
[47] R. R. Coifman, S. Lafon, A. B. Lee, M. Maggioni, B. Nadler, F. Warner, and S. W. Zucker, "Geometric diffusions as a tool for harmonic analysis and structure definition of data: Diffusion maps," Proceedings of the National Academy of Sciences **102**, 7426–7431 (2005).
[48] R. Vos De Wael, O. Benkarim, C. Paquola, S. Lariviere, J. Royer, S. Tavakol, T. Xu, S.-J. Hong, G. Langs, S. Valk, B. Misic, M. Milham, D. Margulies, J. Smallwood, and B. C. Bernhardt, "BrainSpace: a toolbox for the analysis of macroscale gradients in neuroimaging and connectomics datasets," Communications Biology **3**, 103 (2020).
[49] R. A. Bethlehem, C. Paquola, J. Seidlitz, L. Ronan, B. Bernhardt, K. A. Tsvetanov, C.-C. Consortium, *et al.*, "Dispersion of functional gradients across the adult lifespan," Neuroimage **222**, 117299 (2020).
[50] A. I. Luppi, L. Uhrig, J. Tasserie, C. M. Signorelli, E. A. Stamatakis, A. Destexhe, B. Jarraya, and R. Cofre, "Local orchestration of distributed functional patterns supporting loss and restoration of consciousness in the primate brain," Nature communications **15**, 2171 (2024).
[51] Z. Huang, G. A. Mashour, and A. G. Hudetz, "Functional geometry of the cortex encodes dimensions of consciousness," Nature Communications **14**, 72 (2023).
[52] C. Timmermann, L. Roseman, S. Haridas, F. E. Rosas, L. Luan, H. Kettner, J. Martell, D. Erritzoe, E. Tagliazucchi, C. Pallavicini, M. Girn, A. Alamia, R. Leech, D. J. Nutt, and R. L. Carhart-Harris, "Human brain effects of DMT assessed via EEG-fMRI," Proceedings of the National Academy of Sciences **120**, e2218949120 (2023).
[53] M. Girn, L. Roseman, B. Bernhardt, J. Smallwood, R. Carhart-Harris, and R. Nathan Spreng, "Serotonergic psychedelic drugs LSD and psilocybin reduce the hierarchical differentiation of unimodal and transmodal cortex," NeuroImage **256**, 119220 (2022).
[54] A. Zalesky, A. Fornito, and E. T. Bullmore, "Network-based statistic: Identifying differences in brain networks," NeuroImage **53**, 1197–1207 (2010).
[55] A. I. Luppi, P. A. Mediano, F. E. Rosas, J. Allanson, J. Pickard, R. L. Carhart-Harris, G. B. Williams, M. M. Craig, P. Finoia, A. M. Owen, L. Naci, D. K. Menon, D. Bor, and E. A. Stamatakis, "A synergistic workspace for human consciousness revealed by Integrated Information Decomposition," eLife **12**, RP88173 (2024).
[56] V. J. Sydnor, B. Larsen, J. Seidlitz, A. Adebimpe, A. F. Alexander-Bloch, D. S. Bassett, M. A. Bertolero, M. Cieslak, S. Covitz, Y. Fan, R. E. Gur, R. C. Gur, A. P. Mackey, T. M. Moore, D. R. Roalf, R. T. Shinohara, and T. D. Satterthwaite, "Intrinsic activity development unfolds along a sensorimotor–association cortical axis in youth," Nature Neuroscience **26**, 638–649 (2023).
[57] A. C. Luo, V. J. Sydnor, A. Pines, B. Larsen, A. F. Alexander-Bloch, M. Cieslak, S. Covitz, A. A. Chen, N. B. Esper, E. Feczko, A. R. Franco, R. E. Gur, R. C. Gur, A. Houghton, F. Hu, A. S. Keller, G. Kiar, K. Mehta, G. A. Salum, T. Tapera, T. Xu, C. Zhao, T. Salo, D. A. Fair, R. T. Shinohara, M. P. Milham, and T. D. Satterthwaite, "Functional connectivity development along the sensorimotor-association axis enhances the cortical hierarchy," Nature Communications **15**, 3511 (2024).
[58] B. T. Thomas Yeo, F. M. Krienen, J. Sepulcre, M. R. Sabuncu, D. Lashkari, M. Hollinshead, J. L. Roffman, J. W. Smoller, L. Zöllei, J. R. Polimeni, B. Fischl, H. Liu, and R. L. Buckner, "The organization of the human cerebral cortex estimated by intrinsic functional connectivity," Journal of Neurophysiology **106**, 1125–1165 (2011).
[59] R. D. Markello and B. Misic, "Comparing spatial null models for brain maps," NeuroImage **236**, 118052 (2021).
[60] J. B. Burt, M. Helmer, M. Shinn, A. Anticevic, and J. D. Murray, "Generative modeling of brain maps with spatial autocorrelation," NeuroImage **220**, 117038 (2020).
[61] A. Schaefer, R. Kong, E. M. Gordon, T. O. Laumann, X.-N. Zuo, A. J. Holmes, S. B. Eickhoff, and B. T. Yeo, "Local-global parcellation of the human cerebral cortex from intrinsic functional connectivity mri," Cerebral cortex **28**, 3095–3114 (2018).
[62] L. Amaral, X. Wang, Y. Bi, and E. Striem-Amit, "Unraveling the impact of congenital deafness on individual brain organization," eLife **13**, RP96944 (2025).
[63] J. B. Burt, M. Demirtaş, W. J. Eckner, N. M. Navejar, J. L. Ji, W. J. Martin, A. Bernacchia, A. Anticevic, and J. D. Murray, "Hierarchy of transcriptomic specialization across human cortex captured by structural neuroimaging topography," Nature Neuroscience **21**, 1251–1259 (2018).
[64] J. Seidlitz, F. Váša, M. Shinn, R. Romero-Garcia, K. J. Whitaker, P. E. Vértes, K. Wagstyl, P. Kirkpatrick Reardon, L. Clasen, S. Liu, A. Messinger, D. A. Leopold, P. Fonagy, R. J. Dolan, P. B. Jones, I. M. Goodyer, A. Raznahan, and E. T. Bullmore, "Morphometric Similarity Networks Detect Microscale Cortical Organization and Predict Inter-Individual Cognitive Variation," Neuron **97**, 231–247.e7 (2018).
[65] J. Y. Hansen, R. D. Markello, J. W. Vogel, J. Seidlitz, D. Bzdok, and B. Misic, "Mapping gene transcription and neurocognition across human neocortex," Nature Human Behaviour **5**, 1240–1250 (2021).
[66] A. Goulas, J.-P. Changeux, K. Wagstyl, K. Amunts, N. Palomero-Gallagher, and C. C. Hilgetag, "The natural axis of transmitter receptor distribution in the human cerebral cortex," Proceedings of the National Academy of Sciences **118**, e2020574118 (2021).
[67] M. J. Arcaro and M. S. Livingstone, "A hierarchical, retinotopic proto-organization of the primate visual system at birth," Elife **6**, e26196 (2017).
[68] W. J. Park, K. Chang, and I. Fine, "Constraints of cross-modal plasticity within hmt+ following early blindness," Journal of Vision **24**, 195–195 (2024).
[69] I. Anurova, S. Carlson, and J. P. Rauschecker, "Overlapping anatomical networks convey cross-modal suppression in the sighted and coactivation of "visual" and auditory cortex in the blind," Cerebral Cortex **29**, 4863–4876 (2019).
[70] C. M. Bauer, G. V. Hirsch, L. Zajac, B.-B. Koo, O. Collignon, and L. B. Merabet, "Multimodal MR-imaging reveals large-scale structural and functional connectivity

changes in profound early blindness," PLOS ONE **12**, e0173064 (2017).

[71] L. Amaral, P. Thomas, A. Amedi, and E. Striem-Amit, "Longitudinal stability of individual brain plasticity patterns in blindness," Proceedings of the National Academy of Sciences **121**, e2320251121 (2024).

[72] T. R. Makin, J. Scholz, D. Henderson Slater, H. Johansen-Berg, and I. Tracey, "Reassessing cortical reorganization in the primary sensorimotor cortex following arm amputation," Brain **138**, 2140–2146 (2015).

[73] P. R. Roelfsema and F. P. De Lange, "Early Visual Cortex as a Multiscale Cognitive Blackboard," Annual Review of Vision Science **2**, 131–151 (2016).

[74] H. Duymuş, M. Verma, Y. Güçlütürk, M. Öztürk, A. B. Varol, Kurt, T. Gezici, B. F. Akgür, Giray, E. E. Öksüz, and A. A. Farooqui, "The visual cortex in the blind but not the auditory cortex in the deaf becomes multiple-demand regions," Brain **147**, 3624–3637 (2024).

[75] A. Kral and A. Sharma, "Crossmodal plasticity in hearing loss," Trends in Neurosciences **46**, 377–393 (2023).

[76] A. A. Ghazanfar and C. E. Schroeder, "Is neocortex essentially multisensory?" Trends in cognitive sciences **10**, 278–285 (2006).

[77] M. M. Murray, D. J. Lewkowicz, A. Amedi, and M. T. Wallace, "Multisensory processes: a balancing act across the lifespan," Trends in neurosciences **39**, 567–579 (2016).

[78] G. Novembre and G. D. Iannetti, "Towards a unified neural mechanism for reactive adaptive behaviour," Progress in neurobiology **204**, 102115 (2021).

[79] Y. Tian, D. S. Margulies, M. Breakspear, and A. Zalesky, "Topographic organization of the human subcortex unveiled with functional connectivity gradients," Nature neuroscience **23**, 1421–1432 (2020).

[80] B. L. Welch, "The significance of the difference between two means when the population variances are unequal," Biometrika **29**, 350–362 (1938).

[81] Y. Benjamini and Y. Hochberg, "Controlling the False Discovery Rate: A Practical and Powerful Approach to Multiple Testing," Journal of the Royal Statistical Society Series B: Statistical Methodology **57**, 289–300 (1995).

[82] L. V. Hedges, "Distribution theory for glass's estimator of effect size and related estimators," journal of Educational Statistics **6**, 107–128 (1981).

[83] R. Rajimehr, H. Xu, A. Farahani, S. Kornblith, J. Duncan, and R. Desimone, "Functional architecture of cerebral cortex during naturalistic movie watching," Neuron **112**, 4130–4146 (2024).

Supplemental information

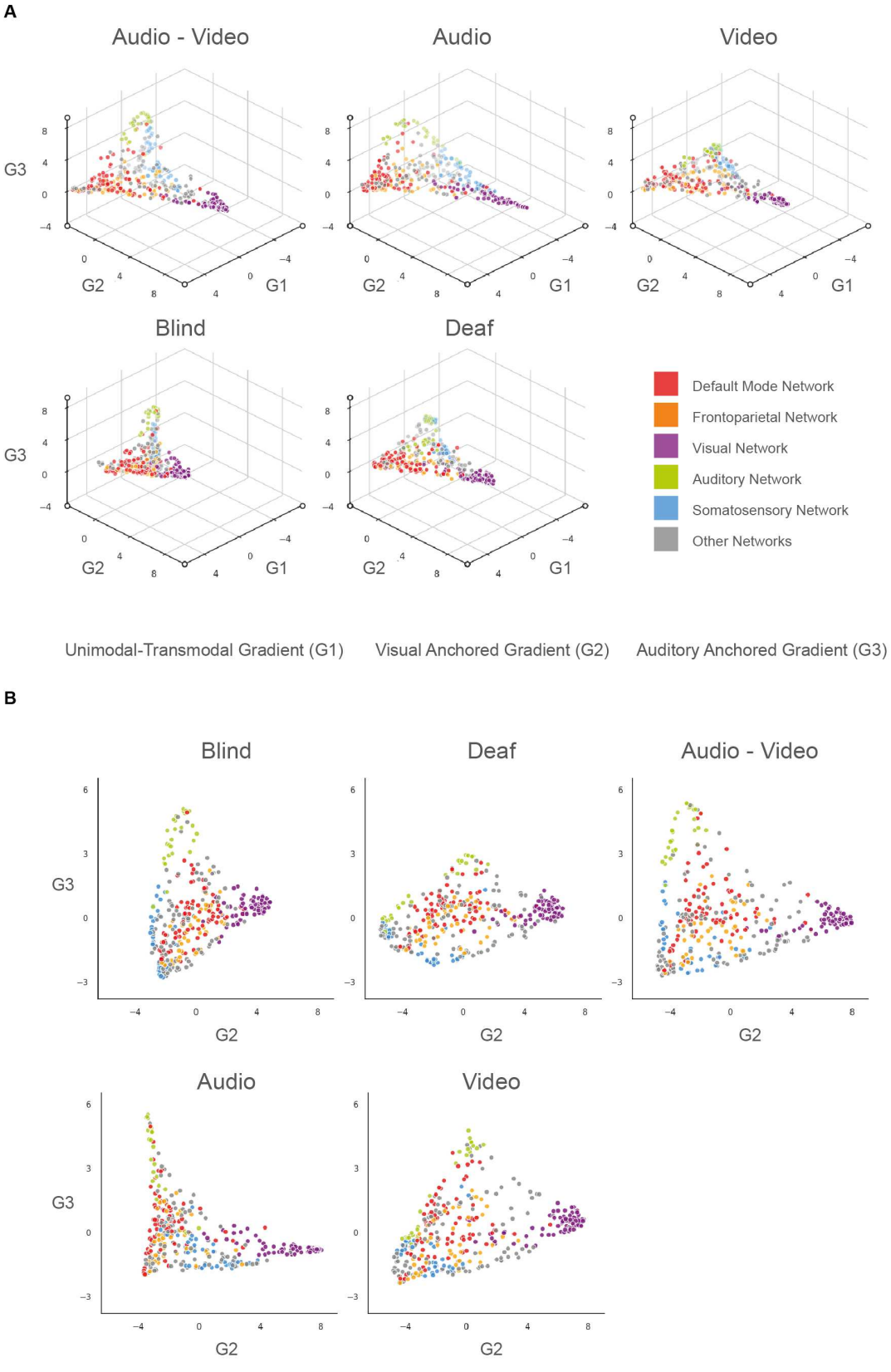

Figure S1. **Diffusion gradient space. A,** Three-dimensional representation of the first three gradients in typically developed individuals under audio-only, visual-only, and audiovisual stimulation. Each point represents a region from the multimodal HCP atlas [7], colored according to its primary functional network. **B,** Two-dimensional representation of the second and third gradients for the same conditions. Each point corresponds to a multimodal HCP atlas [7] region, with colors indicating the associated functional network.

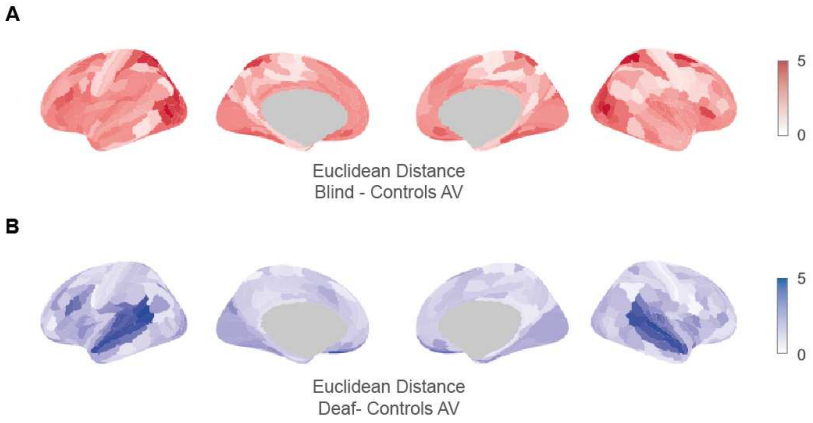

Figure S2. **Regional functional displacement. A,** Mean Euclidean distance in the three-dimensional diffusion embedding space (based on the first three gradients) for each region of the multimodal HCP atlas [7], comparing typically developed individuals under audiovisual stimulation with congenitally blind individuals. **B,** Same analysis as in A, comparing typically developed individuals with congenitally deaf individuals.

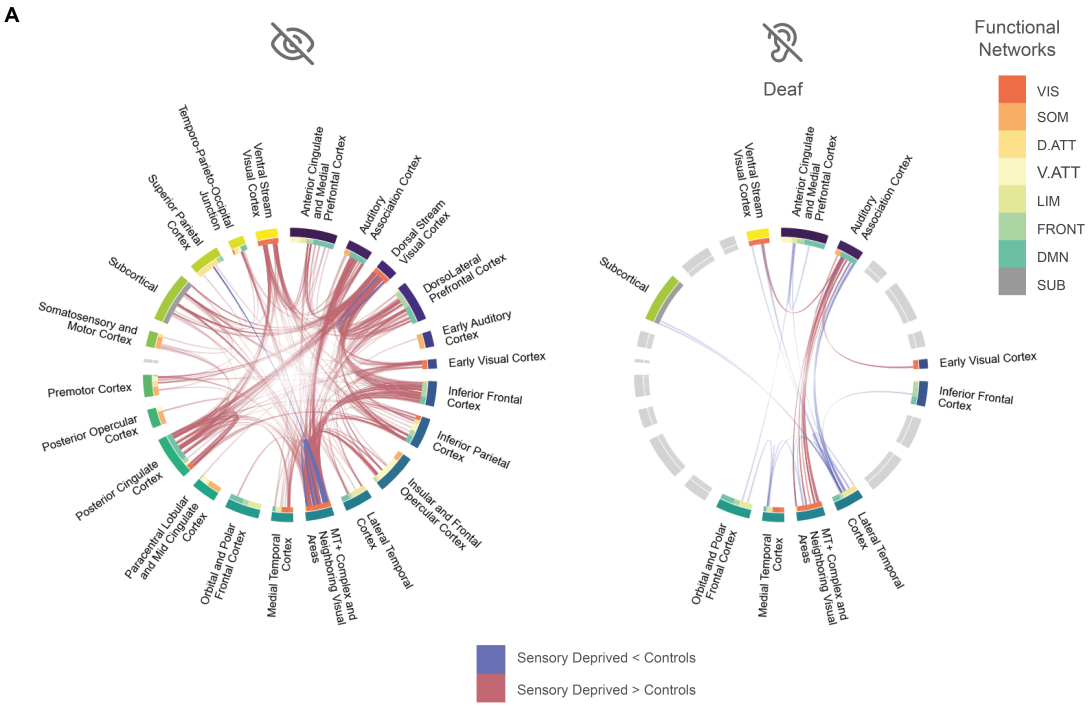

Figure S3. **Group-level differences in whole-brain functional connectivity. A,** Group differences in functional connectivity between congenitally blind or deaf individuals and matched typically developed controls identified using Network-Based Statistics (NBS; F $\geq$ 9, $p < 0.05$). Chord diagrams show significantly increased (blue) and decreased (red) connections for each sensory-deprived group. As in Figure 4, results are shown here according to the macro-anatomical subdivisions of the Glasser atlas. Congenitally blind individuals exhibited increased connectivity between deprived extrastriate visual areas (e.g., MT+ complex and dorsal stream cortices) and frontal regions (dorsolateral and inferior frontal cortex, spanning frontoparietal and DMN networks), alongside decreased intra-visual connectivity. Congenitally deaf individuals showed increased connectivity between visual areas (including MT+ and adjacent regions) and auditory association cortices (e.g., STS, A4, and A5), alongside decreased connectivity mainly between the temporal pole and both the MT+ complex and auditory associa- tion cortices.

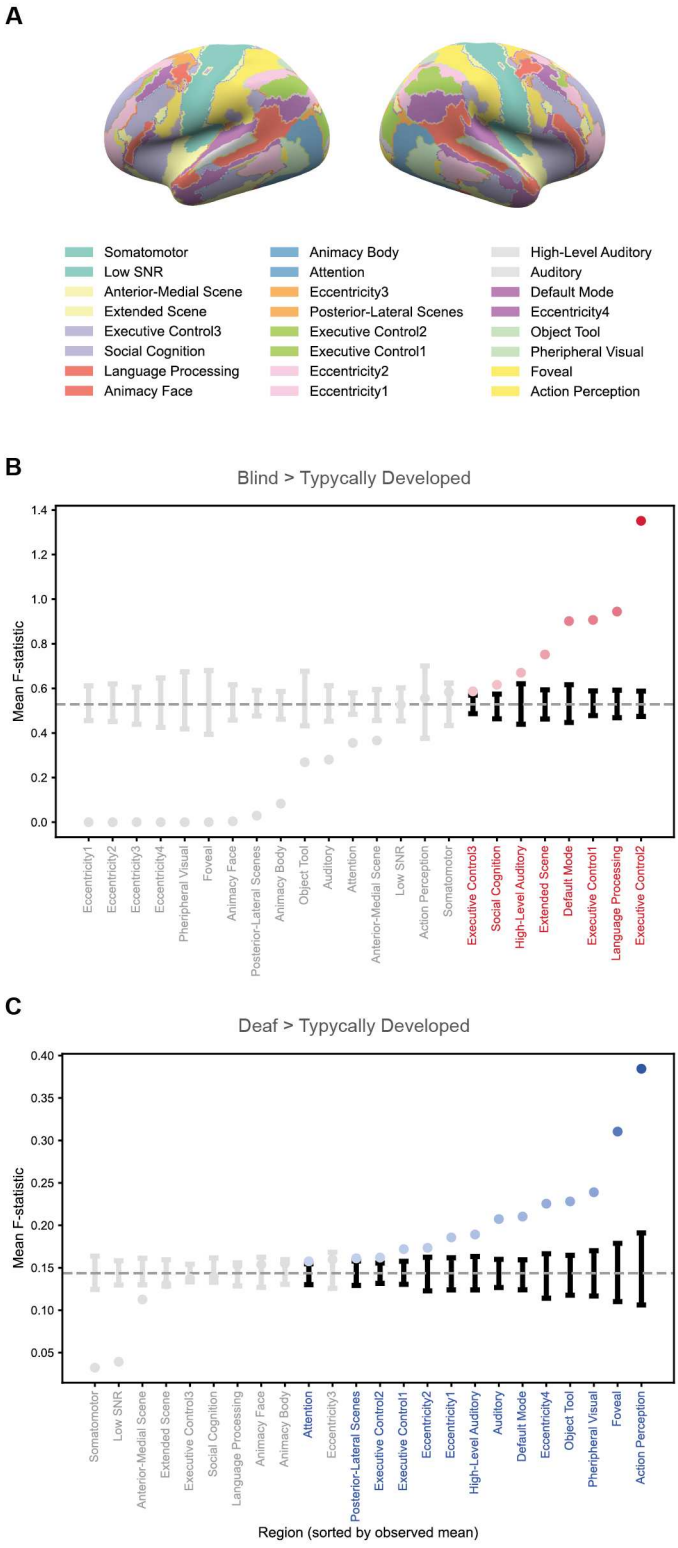

Figure S4. **Regional responses during film-watching across sensory-deprived groups. A,** Inflated cortical surface maps colored according to the functional parcellation defined by Rajimehr *et al.* [83], used to subdivide the cortex into parcels with consistent functional profiles during film viewing. **B, C,** To further characterize group differences observed during the film-watching task, we considered the mean composite F-statistic (as Figure 4) for each cortical region defined by Rajimehr *et al.* [83]. Functional terms are sorted by their observed mean F-statistic. Colored labels highlight regions where observed values exceed the 95th percentile of a null distribution generated from 10,000 spatial-autocorrelation-preserving surrogate maps [60], indicating statistically significant group effects. Grey points fall within the null distribution. Error bars represent the 95% confidence interval of the null distribution for each parcel.

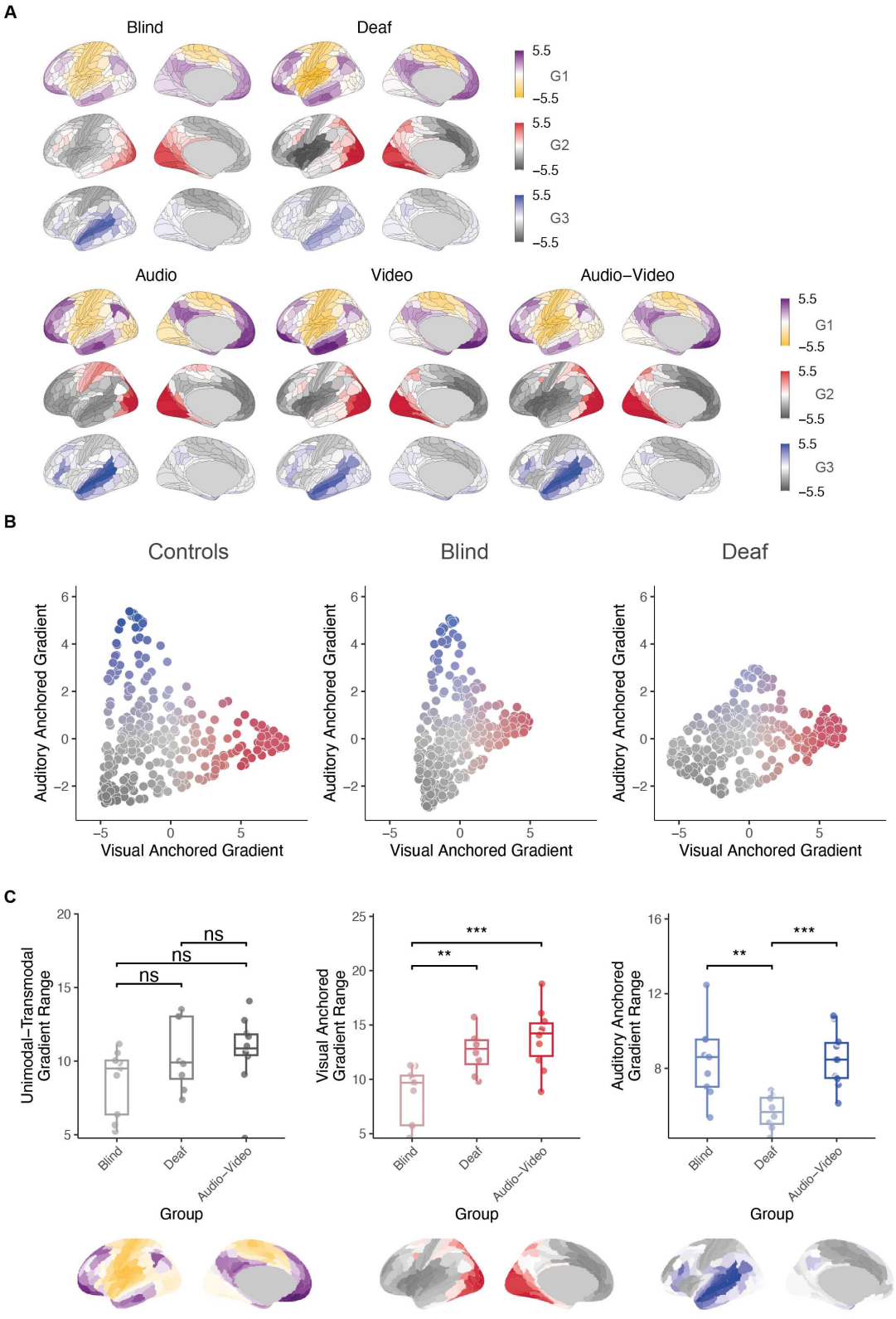

Figure S5. **Topographical maps and functional geometry under sensory deprivation (diffusion parameter $\alpha = 0.3$). A,** Surface maps of the first three cortical gradients in typically developed individuals under audio-only, visual-only, and audiovisual stimulation. Gradient 1 (G1) reflects the principal unimodal-to-transmodal axis, while G2 and G3 are anchored in visual and auditory cortices, respectively. Corresponding gradients in congenitally blind and deaf individuals, averaged across conditions. G1 remains consistent, whereas G2 and G3 show altered spatial structure, reflecting the lack of modality-specific input. **B,** Two-dimensional gradient embeddings illustrate compression along G2 in blind (horizontal arrow) and along G3 in deaf individuals (vertical arrow), relative to the audiovisual condition in controls. **C,** Boxplots show gradient range across groups. G1 does not differ significantly. Blind individuals show reduced G2 range; deaf individuals show reduced G3 range. Statistical tests are two-tailed t-tests (n.s. = not significant; ** $p < 0.01$; ***$p < 0.001$). Gradient topographies are shown below each plot.

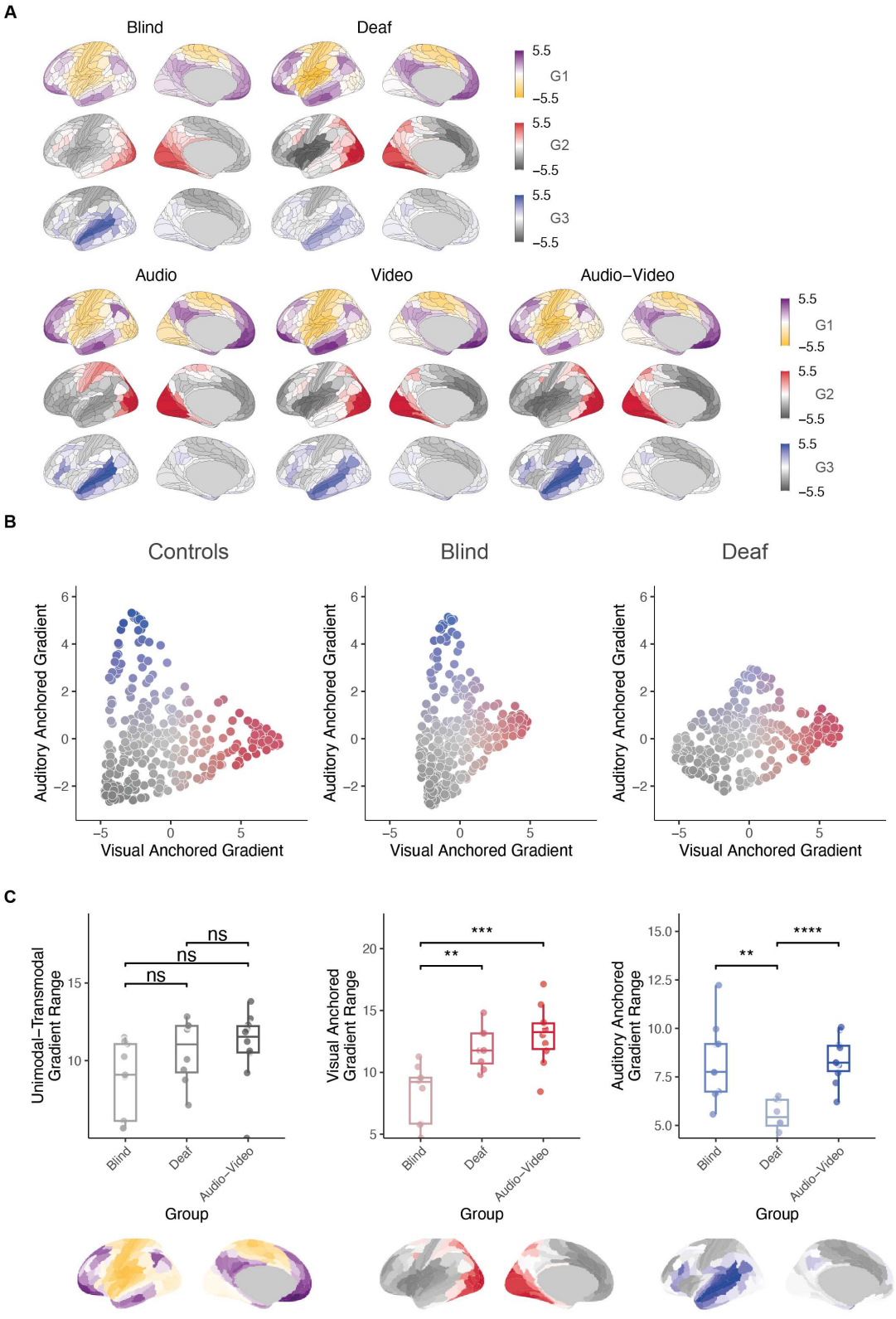

Figure S6. **Topographical maps and functional geometry under sensory deprivation (diffusion parameter $\alpha = 0.7$).A,** Surface maps of the first three cortical gradients in typically developed individuals under audio-only, visual-only, and audiovisual stimulation. Gradient 1 (G1) reflects the principal unimodal-to-transmodal axis, while G2 and G3 are anchored in visual and auditory cortices, respectively. Corresponding gradients in congenitally blind and deaf individuals, averaged across conditions. G1 remains consistent, whereas G2 and G3 show altered spatial structure, reflecting the lack of modality-specific input. **B,** Two-dimensional gradient embeddings illustrate compression along G2 in blind (horizontal arrow) and along G3 in deaf individuals (vertical arrow), relative to the audiovisual condition in controls. **C,** Boxplots show gradient range across groups. G1 does not differ significantly. Blind individuals show reduced G2 range; deaf individuals show reduced G3 range. Statistical tests are two-tailed t-tests (n.s. = not significant; ** $p < 0.01$; ***$p < 0.001$; ****$p < 0.0001$). Gradient topographies are shown below each plot.

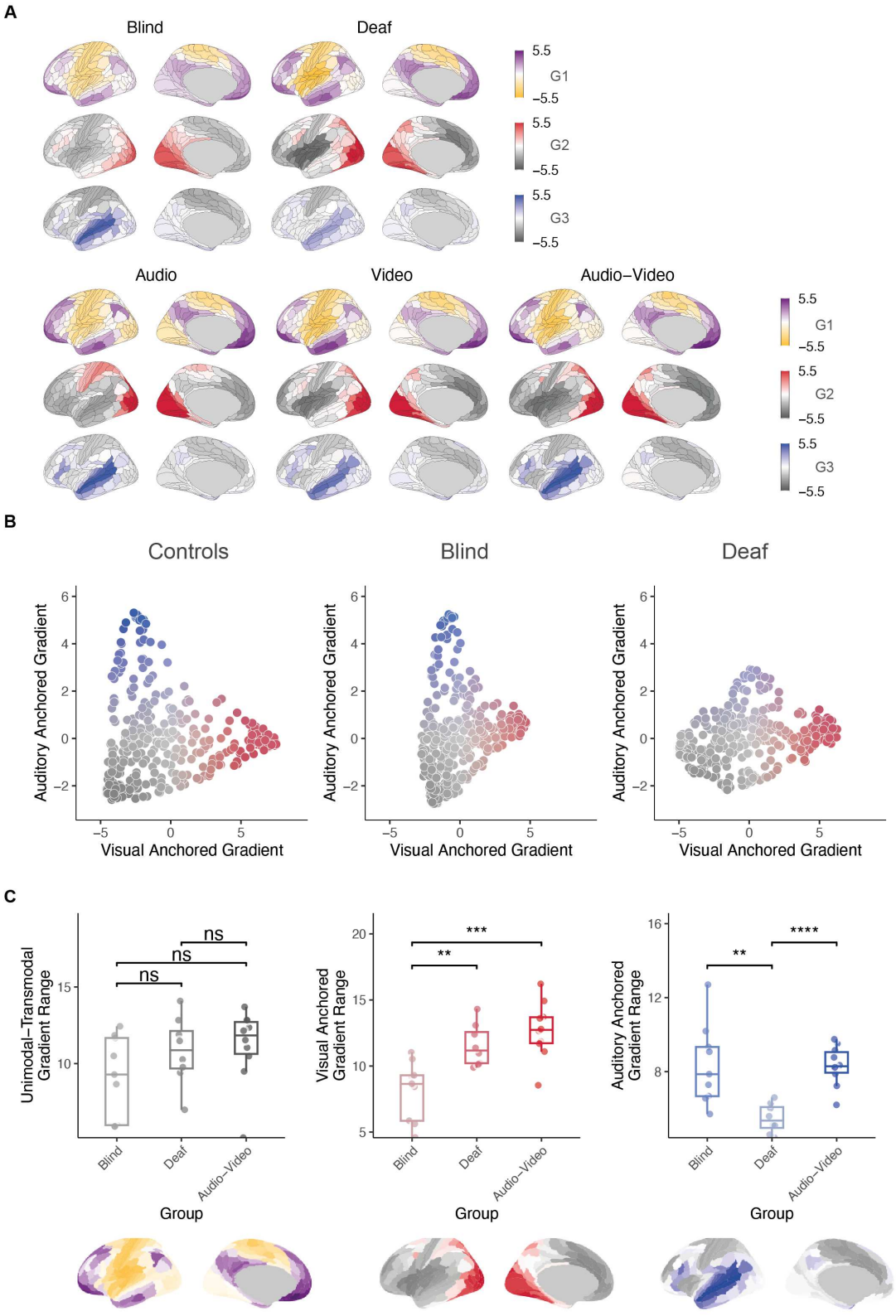

Figure S7. **Topographical maps and functional geometry under sensory deprivation (diffusion parameter $\alpha = 0.9$).A,** Surface maps of the first three cortical gradients in typically developed individuals under audio-only, visual-only, and audiovisual stimulation. Gradient 1 (G1) reflects the principal unimodal-to-transmodal axis, while G2 and G3 are anchored in visual and auditory cortices, respectively. Corresponding gradients in congenitally blind and deaf individuals, averaged across conditions. G1 remains consistent, whereas G2 and G3 show altered spatial structure, reflecting the lack of modality-specific input. **B**, Two-dimensional gradient embeddings illustrate compression along G2 in blind (horizontal arrow) and along G3 in deaf individuals (vertical arrow), relative to the audiovisual condition in controls. **C,** Boxplots show gradient range across groups. G1 does not differ significantly. Blind individuals show reduced G2 range; deaf individuals show reduced G3 range. Statistical tests are two-tailed t-tests (n.s. = not significant; ** $p < 0.01$; ***$p < 0.001$; ****$p < 0.0001$). Gradient topographies are shown below each plot.

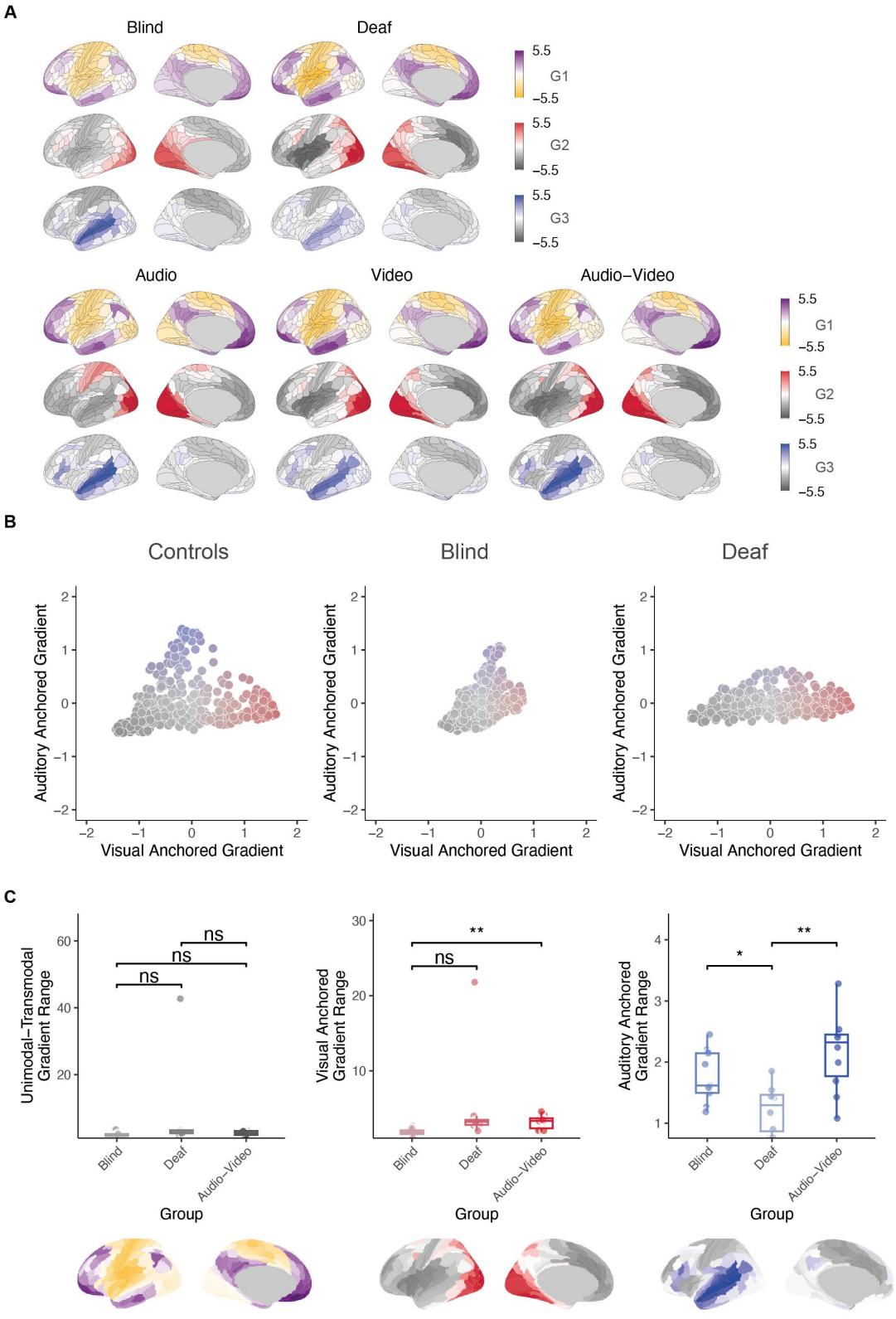

Figure S8. **Topographical maps and functional geometry under sensory deprivation (sparsity $\delta = 70\%$).A,** Surface maps of the first three cortical gradients in typically developed individuals under audio-only, visual-only, and audiovisual stimulation. Gradient 1 (G1) reflects the principal unimodal-to-transmodal axis, while G2 and G3 are anchored in visual and auditory cortices, respectively. Corresponding gradients in congenitally blind and deaf individuals, averaged across conditions. G1 remains consistent, whereas G2 and G3 show altered spatial structure, reflecting the lack of modality-specific input. **B,** Two-dimensional gradient embeddings illustrate compression along G2 in blind (horizontal arrow) and along G3 in deaf individuals (vertical arrow), relative to the audiovisual condition in controls. **C,** Boxplots show gradient range across groups. G1 does not differ significantly. Blind individuals show reduced G2 range; deaf individuals show reduced G3 range. Statistical tests are two-tailed t-tests (n.s. = not significant; *$p < 0.05$; ** $p < 0.01$). Gradient topographies are shown below each plot.

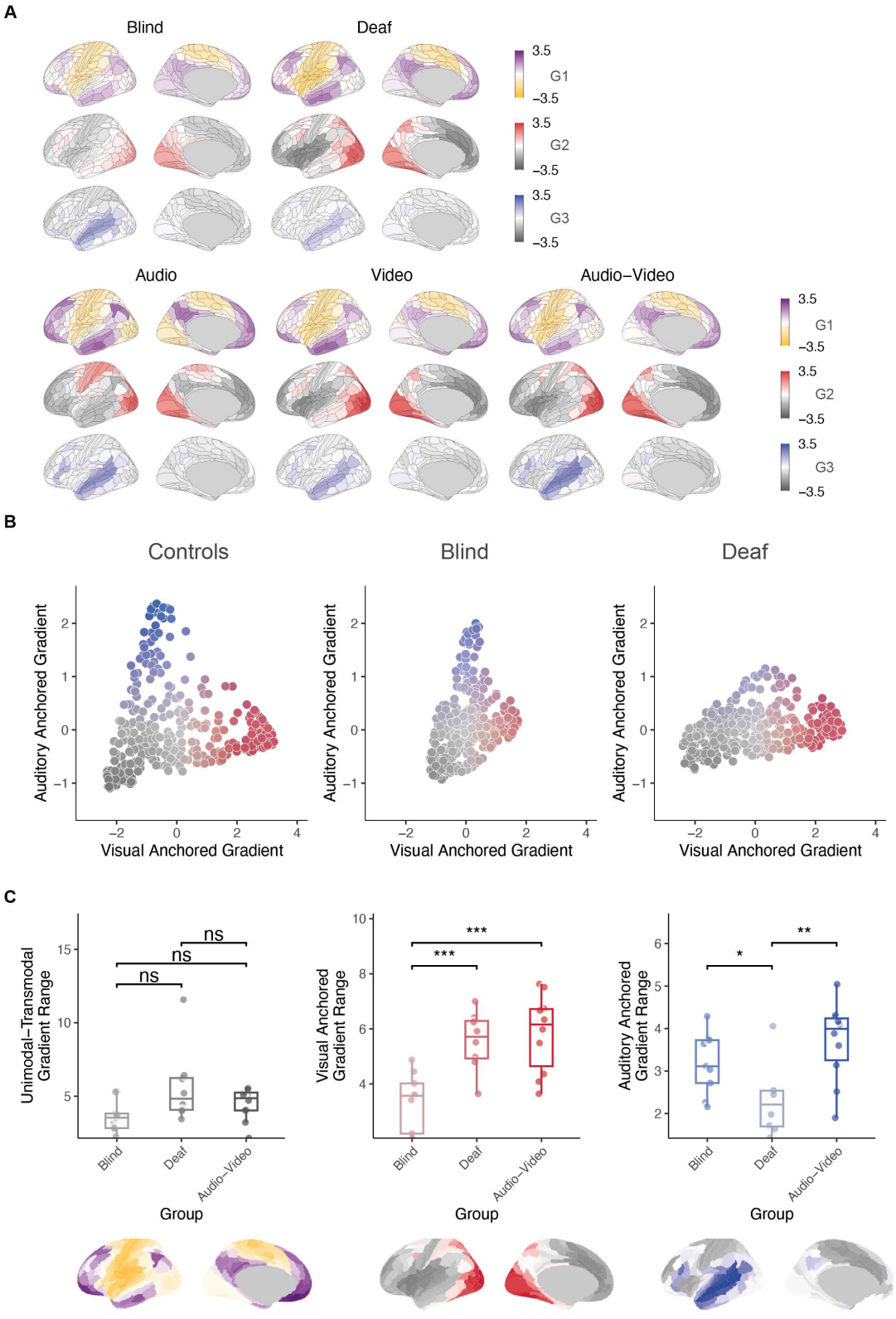

Figure S9. **Topographical maps and functional geometry under sensory deprivation (sparsity $\delta = 80\%$).A,** Surface maps of the first three cortical gradients in typically developed individuals under audio-only, visual-only, and audiovisual stimulation. Gradient 1 (G1) reflects the principal unimodal-to-transmodal axis, while G2 and G3 are anchored in visual and auditory cortices, respectively. Corresponding gradients in congenitally blind and deaf individuals, averaged across conditions. G1 remains consistent, whereas G2 and G3 show altered spatial structure, reflecting the lack of modality-specific input. **B,** Two-dimensional gradient embeddings illustrate compression along G2 in blind (horizontal arrow) and along G3 in deaf individuals (vertical arrow), relative to the audiovisual condition in controls. **C,** Boxplots show gradient range across groups. G1 does not differ significantly. Blind individuals show reduced G2 range; deaf individuals show reduced G3 range. Statistical tests are two-tailed t-tests (n.s. = not significant; *$p < 0.05$; ** $p < 0.01$; *** $p < 0.001$). Gradient topographies are shown below each plot.

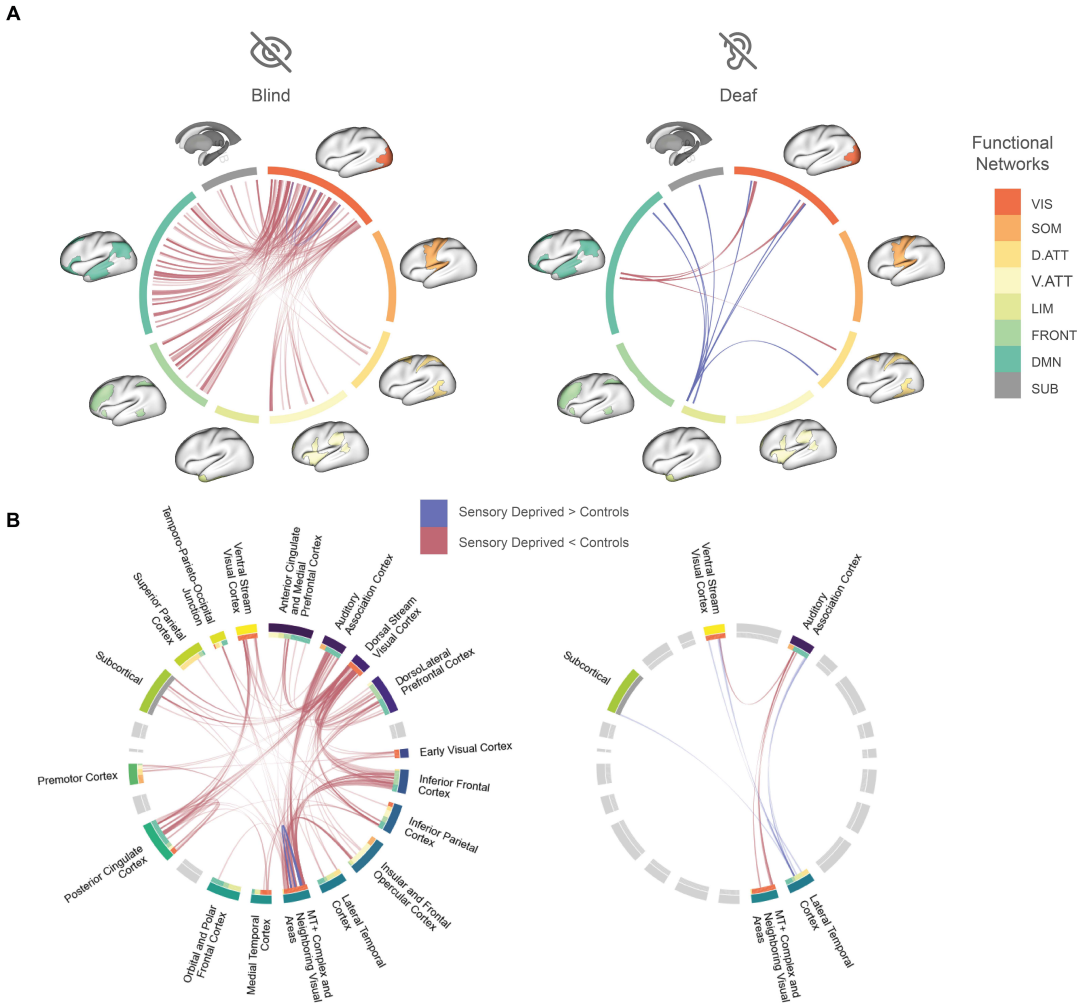

Figure S10. **Group-level differences in whole-brain functional connectivity (F>12). A,** Group differences in functional connectivity between congenitally blind or deaf individuals and matched typically developed controls, identified using Network-Based Statistics with a more stringent threshold (NBS; F $\geq$ 12, $p < 0.05$). Chord diagrams display significantly increased (blue) and decreased (red) connections in each sensory-deprived group. Cortical nodes are grouped according to canonical functional networks [58]: VIS = visual, SOM = somatomotor, D.ATT = dorsal attention, V.ATT = ventral attention, LIM = limbic, FRONT = frontoparietal, DMN = default mode, SUB = subcortical. **B,** The same results are shown using macro-anatomical subdivisions from the Glasser atlas. Congenitally blind individuals exhibit increased connectivity between deprived extrastriate visual areas (e.g., MT+ complex and dorsal stream cortices) and frontal regions (dorsolateral and inferior frontal cortex, spanning frontoparietal and DMN networks), along with decreased intra-visual connectivity. Congenitally deaf individuals show increased connectivity between visual areas (including MT+ and adjacent regions) and auditory association cortices, , alongside decreased connectivity between the temporal pole and auditory associa- tion cortices.

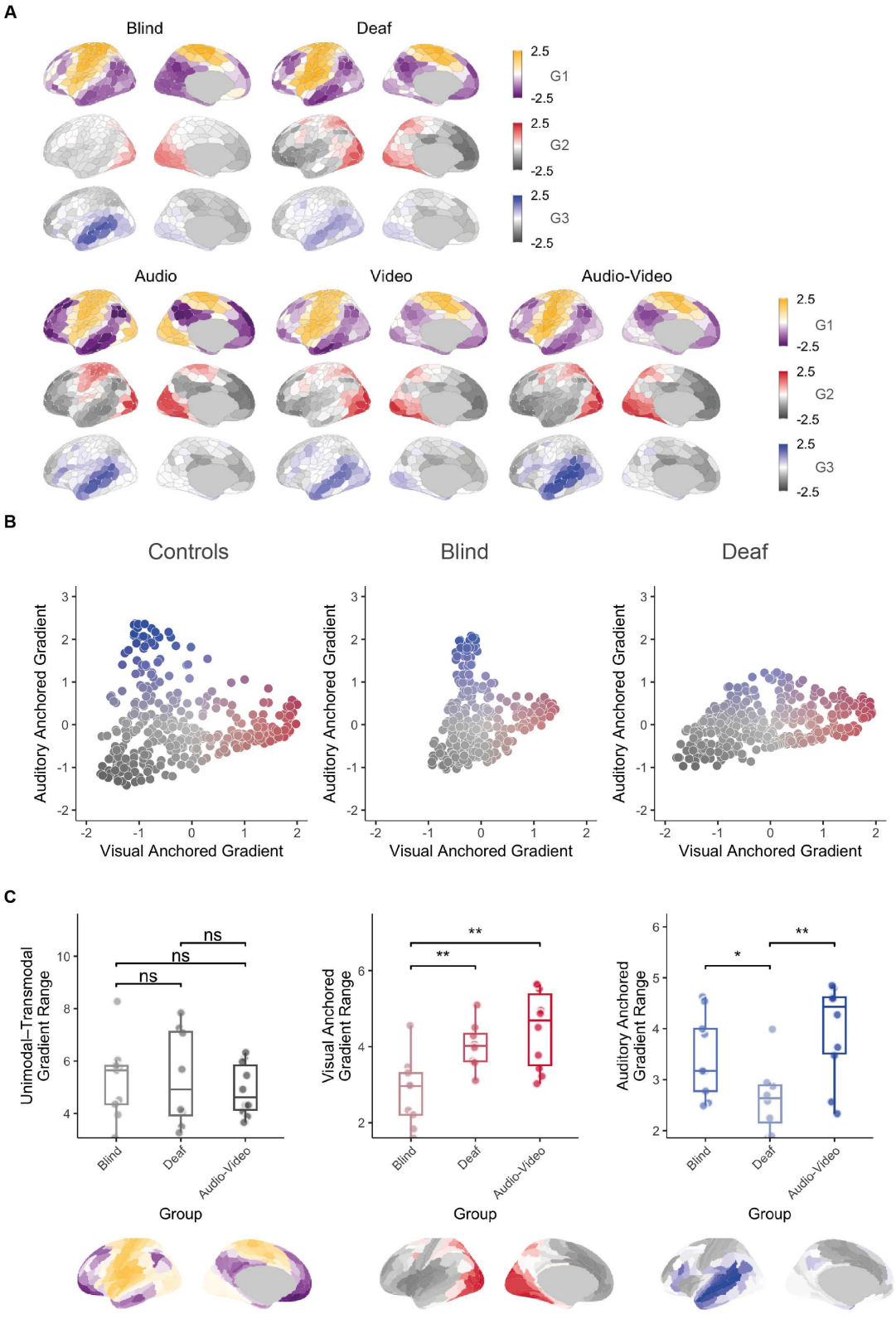

Figure S11. **Topographical maps and functional geometry under sensory deprivation (alternative parcellation Schaefer400).A,** Surface maps of the first three cortical gradients in typically developed individuals under audio-only, visual-only, and audiovisual stimulation. Gradient 1 (G1) reflects the principal unimodal-to-transmodal axis, while G2 and G3 are anchored in visual and auditory cortices, respectively. Corresponding gradients in congenitally blind and deaf individuals, averaged across conditions. G1 remains consistent, whereas G2 and G3 show altered spatial structure, reflecting the lack of modality-specific input. **B,** Two-dimensional gradient embeddings illustrate compression along G2 in blind (horizontal arrow) and along G3 in deaf individuals (vertical arrow), relative to the audiovisual condition in controls. **C,** Boxplots show gradient range across groups. G1 does not differ significantly. Blind individuals show reduced G2 range; deaf individuals show reduced G3 range. Statistical tests are two-tailed t-tests (n.s. = not significant; *$p < 0.05$; ** $p < 0.01$). Gradient topographies are shown below each plot.

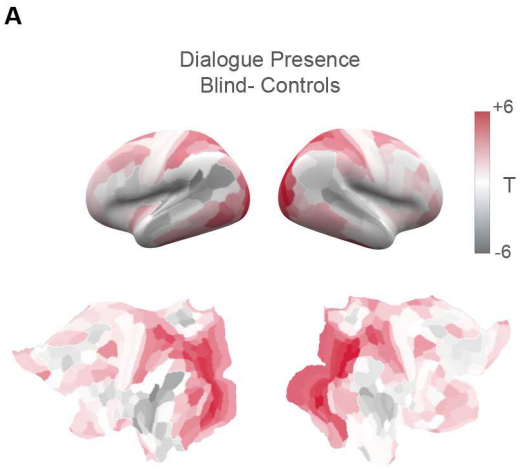

Figure S12. **Feature-specific recruitment of deprived sensory cortices. A,** BOLD time series from each cortical region were correlated with binary time courses of the presence or absence of dialogue. Correlation maps were generated per subject and compared across groups. Surface renderings and inflated ROI maps show results from region-wise two-tailed t-tests contrasting sensory-deprived and typically developed individuals. Blind participants show significantly stronger correlations between speech- related features and visual cortices (red, $p < 0.05$ FDR BH-corrected).